# Synthesis, Characterization and Biological Evaluation of Ureidofibrate-Like Derivatives Endowed with Peroxisome Proliferator-Activated Receptor Activity

L. Porcelli,[†,○] F. Gilardi,[‡,▽,○] A. Laghezza,[§] L. Piemontese,[§] N. Mitro,[‡] A. Azzariti,[†] F. Altieri,[‖]
L. Cervoni,[‖] G. Fracchiolla,[§] M. Giudici,[‡] U. Guerrini,[‡] A. Lavecchia,[⊥] R. Montanari,[#] C. Di Giovanni,[⊥]
A. Paradiso,[†] G. Pochetti,[#] G. M. Simone,[†] P. Tortorella,[§] M. Crestani,*[,‡,○] and F. Loiodice*[,§,○]

[†]Laboratorio di Oncologia Sperimentale Clinica, Istituto Tumori "Giovanni Paolo II", 70124 Bari, Italy

[‡]Dipartimento di Scienze Farmacologiche, Università degli Studi di Milano, 20133 Milano, Italy

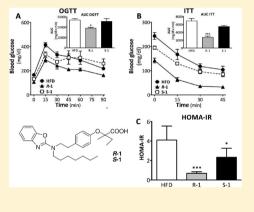[§]Dipartimento Farmaco-Chimico, Università degli Studi di Bari "Aldo Moro", 70126 Bari, Italy

[‖]Dipartimento di Scienze Biochimiche "A. Rossi Fanelli", Università di Roma "La Sapienza", 00185 Roma, Italy

[⊥]Dipartimento di Chimica Farmaceutica e Tossicologica, Università di Napoli "Federico II", 80131 Napoli, Italy

[#]Istituto di Cristallografia, Consiglio Nazionale delle Ricerche, Montelibretti, 00015 Monterotondo Stazione, Roma, Italy

**S** *Supporting Information*

**ABSTRACT:** A series of ureidofibrate-like derivatives was prepared and assayed for their PPAR functional activity. A calorimetric approach was used to characterize PPARγ−ligand interactions, and docking experiments and X-ray studies were performed to explain the observed potency and efficacy. *R*-1 and *S*-1 were selected to evaluate several aspects of their biological activity. In an adipogenic assay, both enantiomers increased the expression of PPARγ target genes and promoted the differentiation of 3T3-L1 fibroblasts to adipocytes. In vivo administration of these compounds to insulin resistant C57Bl/6J mice fed a high fat diet reduced visceral fat content and body weight. Examination of different metabolic parameters showed that *R*-1 and *S*-1 are insulin sensitizers. Notably, they also enhanced the expression of hepatic PPARα target genes indicating that their in vivo effects stemmed from an activation of both PPARα and γ. Finally, the capability of *R*-1 and *S*-1 to inhibit cellular proliferation in colon cancer cell lines was also evaluated.

## ■ INTRODUCTION

PPARs are ligand-dependent transcription factors belonging to the nuclear receptor superfamily. They control the expression of genes involved in fatty acid and glucose metabolism and function as cellular lipid sensors that activate transcription in response to the binding of a cognate ligand, generally fatty acids and their eicosanoids metabolites.[1−3] As ligand-dependent receptors, PPARs form heterodimers with the Retinoid X Receptor (RXR) and adopt an active conformation in the presence of a ligand. Additional coregulator proteins are recruited to create a complex that binds to Peroxisome Proliferator Response Elements (PPRE) in target genes and regulates their expression.[4−6]
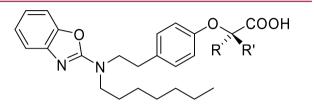
Three main PPAR subtypes have been identified: PPARα (NR1C1), PPARβ (also known as PPARδ) (NR1C2), and PPARγ (NR1C3). PPARα is mainly expressed in the liver and activates a genetic program leading to fatty acid β-oxidation. PPARβ is more ubiquitously distributed and regulates cellular functions such as fatty acid catabolism in the skeletal muscle, wound healing, and inflammation. PPARγ plays important roles in the differentiation and functions of adipocytes and macrophages with a direct impact on type 2 diabetes,

dyslipidemia, atherosclerosis, and cardiovascular diseases.[7,8] This receptor subtype is the target of the thiazolidinedione class of antidiabetic agents (TZDs). TZDs are PPARγ agonists whose insulin-sensitizing action is well established.[9] However, as full agonists they also stimulate adipocyte differentiation in vitro and weight gain in vivo, which normally aggravates the diabetic state. Additional undesirable side effects associated with TZD treatment include fluid retention, edema/hemodilution, cardiomegaly, anemia, and increased incidence of bone fractures.[10,11] As a result of the clinical observations mentioned above, emphasis has shifted to the development of partial agonists or selective PPARγ modulators (SPPARγMs). The SPPARM approach has recently attracted considerable attention because it proposes that diverse PPAR ligands, depending on their chemical structures, would bind in a distinct manner to PPARs inducing different levels of activation and distinct conformational changes of the receptor, leading to differential interactions with coactivators and corepressors.

Structurally diverse modulators or partial agonists, therefore, are likely to elicit different pharmacological and toxicological effects depending on the context of tissue, i.e., abundance of cofactor proteins and target gene. This may enable uncoupling of the benefits of PPAR activation from the adverse effects associated with full agonism. In agreement with the SPPARγM concept, a number of these modulators have already demonstrated desirable pharmacological profiles in various rodent models with significantly reduced side effects relative to those generally observed with existing full agonists.[12−24]

In a previous work,[25] we reported a structural study on two enantiomeric ureidofibrate-like derivatives (Figure 1) complexed,



**1-5**

| Compound | R | R' |
|----------|-----|------|
| R-1 | $CH_3$ | $C_2H_5$ |
| S-1 | $C_2H_5$ | $CH_3$ |
| 2 | $CH_3$ | $CH_3$ |
| R-3 | H | $CH_3$ |
| S-3 | $CH_3$ | H |
| 4 | H | H |
| R-5 | H | $CH_2Ph$ |
| S-5 | $CH_2Ph$ | H |

**Figure 1.** Ureidofibrate-like derivatives of the present study.

respectively, with the ligand binding domain (LBD) of PPARγ. The R-enantiomer, **R-1**, behaves as a full agonist of PPARγ whereas the S-enantiomer, **S-1**, is a less potent partial agonist. Comparing the X-ray structures of the two complexes we argued that the partial agonist behavior of **S-1** could be ascribed to a destabilization of the active conformation of helix 12 (H12). In particular, we showed that the suboptimal conformation of H12, observed in the PPARγ/**S-1** complex, is probably due to a steric hindrance between the ethyl group, linked to the asymmetric carbon atom of the ligand, and the crucial residue Q286 of PPARγ, situated on helix 3 (H3). The importance of the residue Q286 on the transcriptional activity of the receptor was tested by site-directed mutagenesis which confirmed its key role in the stabilization of helix 12.[26] The functional relevance of this residue in determining the receptor activity of these enantiomeric ureidofibrate-like derivatives, prompted us to investigate the possibility to fine tune the activity of these ligands by modifying the substituents bound to the stereogenic center at the α position of the carboxylic group. In this work we report, therefore, the synthesis and PPARγ functional activity of derivatives **2−5** (Figure 1) in which shorter or longer substituents were introduced in place of the methyl and/or ethyl of **R-1** and **S-1**. The functional
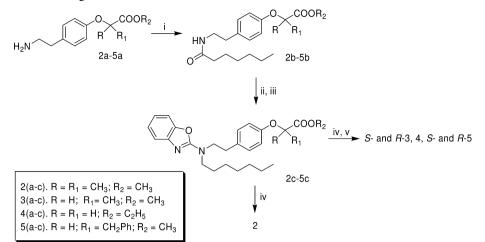
activity of these compounds toward PPARγ, as well as PPARα and PPARβ/δ, was determined by the transactivation assay in transiently transfected human hepatoblastoma cell line HepG2 or the monkey kidney cell line COS-1. Moreover, we decided to use a calorimetric approach (ITC, DSC) to characterize PPARγ−ligand interactions including the binding affinity. As far as we know, this is the first case in which calorimetric techniques have been applied to a series of structurally related PPARγ ligands for the determination of the thermodynamic parameters associated with the formation of the receptor−ligand complexes. On the basis of these results, docking experiments and X-ray studies were performed to provide a molecular explanation for their different potency and efficacy. In addition, we evaluated several aspects of the activity of **R-1** and **S-1**. First of all, we tested the adipogenic activity of **R-1** and **S-1** in 3T3-L1 adipocytes and then explored their in vivo pharmacological properties in a mouse model of obesity and insulin resistance to study the activity of these compounds on typical PPARα and PPARγ targets.

Finally, since a large body of evidence shows that PPARγ ligands exert antitumorigenic effects against a wide variety of neoplastic cells both in vivo and in vitro,[27−31] we evaluated the capability of the two enantiomers **R-1** and **S-1** to inhibit cellular proliferation in colon cancer cell lines. However, we found that the antiproliferative activity exhibited by these ligands was only partially related to PPARγ activation.

**Chemistry.** The synthesis of compounds **2−5**, which followed the procedure previously reported for the preparation of **R-1** and **S-1**,[26] is depicted in Scheme 1 and involved the key amine intermediates **2a−5a** whose condensation with hepta-noic acid in the presence of hydroxybenzotriazole (HOBT) and N,N-diisopropylcarbodiimide (DIC) afforded the correspond-ing amide intermediates **2b−5b**. The amide group of these intermediates was reduced with 1 M borane in THF solution to give the corresponding amines. The condensation with 2-chloro-benzoxazole, followed by saponification of the ester function, led to the final acids **2−5**. All acids, except **2**, were obtained as colorless oils, which were transformed into sodium (**R-3**, **S-3**, and **4**) or cyclohexylamine salts (**R-5** and **S-5**) before undergoing the biological assay. The synthetic pathways of key amine intermediates **2a−5a** are reported in Scheme 2. The synthesis of **2a** involved the ethyl ester intermediate **2d**, which was prepared by reaction of 4-bromo-phenol with acetone in the presence of $CHBr_3$ and KOH. The condensation of this compound with N-vinylphthalimide in the presence of $Pd(AcO)_2$, tri-o-tolylphosphine and N,N-diisopropylethylamine in anhydrous $CH_3CN$, followed by hydrogenation at 4 atm in the presence of Wilkinson catalyst, provided compound **2e**. The hydrazinolysis of the phthalimide moiety led to the desired amine intermediate. Following the same procedure, both enantiomers of compound **5a** were prepared starting from **R-** and **S-5d**, which were obtained from the condensation of 4-bromo-phenol with S- or R-methylphenyllactate, respectively, under Mitsunobu conditions. The amines **3a** and **4a** were prepared starting from the commercially available tiramine, which was condensed with carbobenzyloxychloride in the presence of $K_2CO_3$ to afford the N-carbobenzyloxytiramine. The condensation of this intermediate with R- or S-ethyl-lactate under Mitsunobu conditions afforded S- or R-3d, respectively, whereas its condensation with ethyl 2-bromoacetate in the presence of 95% NaH powder in anhydrous DMF provided the intermediate **4d**. The hydrogenation of S- or R-3d and **4d** at 5 atm in the presence of 10% Pd/C in EtOH led to the desired amines.
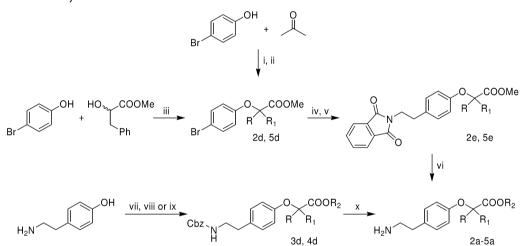
**Scheme 1. Synthesis of PPAR Agonists 2−5**[a]



2(a-c). R = R₁ = CH₃; R₂ = CH₃
3(a-c). R = H; R₁ = CH₃; R₂ = CH₃
4(a-c). R = R₁ = H; R₂ = C₂H₅
5(a-c). R = H; R₁ = CH₂Ph; R₂ = CH₃

[a](i) Heptanoic acid, HOBT, DIC, CH₂Cl₂; (ii) 1 M BH₃ in THF; (iii) 2-chloro-benzoxazole, (Et)₃N, THF; (iv) 1 N NaOH, EtOH, rt; (v) NaHCO₃ (for compounds 3 and 4) or cyclohexylamine (for compound 5), EtOH, rt.

**Scheme 2. Synthesis of Key Amine Intermediates 2a−5a**[a]



[a](i) CHBr₃, KOH; (ii) MeOH, H₂SO₄ cat.; (iii) DIAD, Ph₃P, anhydrous toluene; (iv) N-vinylphthalimide, Pd(AcO)₂, tri-o-tolylphosphine, N,N-diisopropylethylamine, CH₃CN; (v) H₂ (4 atm), Wilkinson cat., EtOH, rt; (vi) N₂H₄·xH₂O, EtOH; (vii) Cbz-Cl, K₂CO₃, EtOH/H₂O; (viii) ethyl 2-bromoacetate, 95% NaH, anhydrous DMF; (ix) R- or S-methyllactate, DIAD, Ph₃P, anhydrous toluene; (x) H₂ (5 atm), 10% Pd/C, EtOH.

Both enantiomers of acids 3 and 5 had enantiomeric excesses ≥95% as determined by HPLC analysis of the chiral stationary phase (see Supporting Information).

### ■ RESULTS AND DISCUSSION

**PPAR Activity.** Compounds 2−5 were evaluated first for their agonist activity on the human PPARγ (hPPARγ) subtype in comparison with R-1 and S-1. For this purpose, the GAL4-PPARγ chimeric receptor was expressed in transiently transfected HepG2 cells according to a previously reported procedure.[32] The results obtained are reported in Table 1 together with corresponding data for rosiglitazone used as a reference compound in the transactivation assay. The maximum induction obtained with the reference agonist was defined as 100%.

Interestingly, all new ligands were PPARγ activators even though with an intrinsic activity significantly lower than that of the full agonist R-1. The substitution of the ethyl group bound to the stereogenic center of 1 with a methyl afforded the achiral compound 2, which exhibited potency similar to that of R-1

and about five times higher than that of S-1. The introduction of a hydrogen in place of the same ethyl group gave compound 3 whose enantiomers showed stereoselective activity with R-3 about 15 times more potent than S-3, even though it was 2 times less potent than R-1. A quite good activity was obtained also with the achiral compound 4 characterized by the presence of a methylene between the phenolic oxygen and the carboxylic function; this analogue, in fact, was only 11 times less potent than R-1. Finally, the two stereoisomers of compound 5 were tested; this derivative was investigated by analogy with previously reported phenoxyalkanoic acid PPAR agonists bearing a benzyl group at α position of the carboxylic group.[32−35] Both R-5 and S-5 displayed a fairly good potency although with the lowest efficacy of the series. For this compound, a small stereoselectivity favorable to the S-isomer was observed.

In order to obtain a more complete pharmacological characterization, compounds 2−5 were evaluated also for their agonist activity on human PPARα and PPARβ/δ subtypes. R-1 and S-1 were assayed only on PPARα given their previously reported inactivity on the PPARβ/δ subtype.[25] The results obtained are

**Table 1. Activity of the Tested Compounds in Cell-Based Transactivation Assay[a]**

| compd | PPAR$\alpha$ | | PPAR$\gamma$ | | PPAR$\delta$ | |
|---|---|---|---|---|---|---|
| | EC$_{50}$ ($\mu$M) | E$_{max}$ (%) | EC$_{50}$ ($\mu$M) | E$_{max}$ (%) | EC$_{50}$ ($\mu$M) | E$_{max}$ (%) |
| **R-1** | 0.003 ± 0.001 | 91 ± 3 | 0.07 ± 0.05[b] | 116 ± 9[b] | ia | ia |
| **S-1** | 0.056 ± 0.034 | 75 ± 4 | 0.59 ± 0.11[b] | 50 ± 5[b] | ia | ia |
| **2** | 0.030 ± 0.016 | 82 ± 7 | 0.11 ± 0.06 | 50 ± 4 | 0.09 ± 0.05 | 83 ± 24 |
| **R-3** | 0.025 ± 0.017 | 93 ± 6 | 0.15 ± 0.06 | 59 ± 2 | 0.13 ± 0.09 | 41 ± 10 |
| **S-3** | 0.620 ± 0.260 | 78 ± 4 | 2.30 ± 1.00 | 32 ± 5 | 0.85 ± 0.14 | 35 ± 7 |
| **4** | 0.122 ± 0.058 | 87 ± 7 | 0.80 ± 0.40 | 37 ± 11 | 0.57 ± 0.07 | 40 ± 11 |
| **R-5** | 1.720 ± 0.950 | 26 ± 7 | 2.70 ± 1.00 | 23 ± 9 | ia | ia |
| **S-5** | ia | ia | 1.70 ± 0.80 | 31 ± 21 | ia | ia |
| Wy-14,643 | 1.6 ± 0.3 | 100 ± 10 | ia | ia | ia | ia |
| rosiglitazone | ia | ia | 0.02 ± 0.01 | 100 ± 21 | ia | ia |
| L-165,041 | ia | ia | ia | ia | 0.021 ± 0.01 | 100 ± 4 |

[a]Efficacy values were calculated as a percentage of the maximum obtained fold induction with the reference compounds. [b]These values correspond to those previously obtained as reported in ref 25.

provided in Table 1 together with corresponding data for pirinixic acid (Wy-14,643) and 4-[3-(4-acetyl-3-hydroxy-2-propylphenoxy)-propoxy]phenoxyacetic acid (L-165,041) used as reference compounds for PPAR$\alpha$ and PPAR$\beta/\delta$, respectively. Interestingly, compounds **2–4** turned out to be pan-agonists basically displaying on both of these receptors the same rank order of activity and stereoselectivity shown for PPAR$\gamma$. They acted as potent full agonists on PPAR$\alpha$, as well as **R-1** and **S-1**, whereas they exhibited lower potency and efficacy on PPAR$\beta/\delta$. On the contrary, **R-5** was inactive on PPAR$\beta/\delta$ while displaying a moderate activity on PPAR$\alpha$; last, **S-5** behaved as the only selective PPAR$\gamma$ agonist of the series. Thus, all of the fibrate analogues (except for **S-5**) were more potent on PPAR$\alpha$ than PPAR$\gamma$. It is worth noting that PPAR$\beta/\delta$ activity was shown only from the compounds with no or small substituents in the $\alpha$ position of the carboxylic group confirming what is already reported in the literature for related fibrate analogues. No PPAR$\beta/\delta$ activity, instead, was observed for derivatives **1** and **5** endowed with bulkier substituents in the same position.

**Calorimetric Measurements.** To investigate the possibility of using the calorimetric approach for the characterization of protein−ligand interactions of PPAR ligands, we decided to use calorimetric techniques to measure the thermodynamic parameters associated with the formation of the complexes between ligands **1–4** and PPAR$\gamma$. Compounds **R-5** and **S-5** were not tested because of the very low solubility of their cyclohexylamine salts in the buffer used for the experiments.

Figure 2 shows the differential scanning calorimetry (DSC) thermograms of PPAR$\gamma$-LBD in the presence and absence of the ligands. In these curves, the heat capacity is reported as a function of temperature with the peaks corresponding to the protein denaturation. The experimental data showed that ligand binding, with the only exception of compound **4**, shifted the denaturation peak by about 2−5 °C. As thermal denaturation was not reversible under these conditions, the DSC thermograms did not yield useful values of $\Delta H$; however, they provided useful hints on the degree of global stabilization of the ligand binding domain of PPAR$\gamma$ from the tested ligands. As known, a global stabilization of PPAR$\gamma$-LBD also has a favorable effect on the transactivation activity because of the indirect stabilization of the activation−function helix 12. Interestingly, the full agonist **R-1** stabilized the receptor better than the reference compound rosiglitazone, even though this did not turn out to be beneficial for increasing the potency.
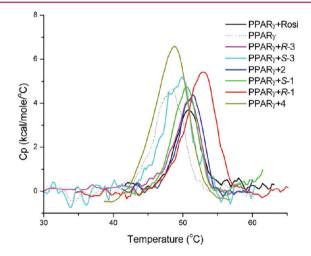


**Figure 2.** DSC thermograms of PPAR$\gamma$-LBD in the presence and absence of the ligands of the present study.

The next step was the determination of thermodynamic parameters relating to the formation of the complexes PPAR$\gamma$-LBD/ligand by isothermal titration calorimetry (ITC). This technique, by measuring the heat absorbed or released by titrating the protein with a ligand at constant temperature, yields the stoichiometry of the reaction, the binding enthalpy, and the affinity constant.

The result of a typical ITC experiment is shown in Figure 3 for binding of **R-3**. In the upper panel, the heat pulses observed upon addition of the ligand to PPAR$\gamma$ are plotted as a function of the injection order. The area of the pulses decreases progressively until it reaches a constant value due to complete saturation of the receptor binding sites. The lower panel shows the integrated heats of reaction plotted against the molar ratio of total ligand concentration to total oligomeric protein concentration, and, superimposed, the simulated curve obtained by the best fitting of the data according to the "one binding site" model. The stoichiometry of ligand binding was generally as expected, with the low accuracy of some results probably due to errors in the active protein concentration.

Table 2 shows that both $\Delta H$ and $T\Delta S$ values for tested compounds **1–4** were favorable to the binding to PPAR$\gamma$ isoform. The association of the ligands was enthalpy-driven at 25 °C, showing that van der Waals interactions and H-bonds played an important role in the binding. The only exception
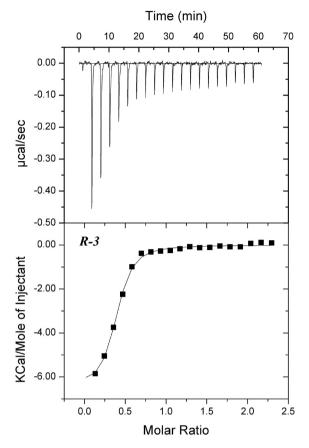
**Figure 3.** Binding of **R-3** to PPARγ-LBD. The upper panel shows the raw data of a representative ITC experiment. The lower panel shows the corresponding binding isotherm fitted according to the "one binding site" model.

As far as the binding affinity was concerned, the results ($K_d$) for **R-1**, **S-1**, and rosiglitazone were in good accordance with the previously reported data of $K_i$ obtained by the scintillation proximity assay (SPA), that is, 0.088 μM, 0.971 μM, and 0.074 μM, respectively.[25] Importantly, the affinity data for the enantiomers of compound **3** confirmed a stereoselectivity favorable to the R-isomer. Thus, the ITC technique could represent a very useful alternative to SPA given that it avoids the use of radio-ligands and is less costly.

**Molecular Modeling and X-ray Studies.** The analysis of the binding affinity of achiral compounds **2** and **4** showed that their $K_d$ values did not correlate well with the activity. Ligand **2**, in particular, was one of the most potent agonists of the series despite its low affinity. To gain more details on the interactions of PPARγ with the partial agonists **S-1**, **2**, and **4** endowed with different potency, an approach that combined molecular docking and X-ray studies was performed.

To this end, the crystal structure of the PPARγ complexed with the ligand **2** was solved (PDB code: 3R8I) and successively compared to that of the complexes PPARγ/**R-1**[25] (PDB code: 2I4J) and PPARγ/**S-1**[25] (PDB code: 2I4P). Interestingly, the analysis of the structures revealed three different orientations of the carboxylate group that can be ascribed only to the differences of the substituents on the carbon atom in α position. As illustrated in Figure 4a, both oxygens of the carboxylate group of **2** are involved in H-bonds with Y473, H323, and H449. This arrangement is more similar to the canonical H-bonding network realized by the potent full agonist **R-1** (Figure 4b), which also has both oxygens engaged in H-bonds with the triad. On the contrary, only one oxygen of **S-1** (Figure 4c) is engaged in H-bonds with the above residues because of the steric clash between the ethyl group on the asymmetric carbon atom and the residue Q286 on helix 3 that forced the ligand to move away from helix 12 provoking a distorted and less efficacious interaction with this helix.[25] Moreover, **2** lacks the H-bond with S289, whereas its benzoxazole N atom establishes a H-bond with C285 of helix 3. A water molecule creates a H-bridge between the benzoxazole O atom and the NH backbone of S342 belonging to the β-sheet. Further hydrophobic contacts with the β-sheet of the receptor are realized by the long aliphatic chain of **2**.

To predict the plausible interactions between compound **4** and PPARγ, molecular docking studies were carried out using the crystal structure of PPARγ/**2** complex. The ligand—receptor complex was predicted through the automated docking software GOLD 5.0.1,[36] which in several studies was shown to yield better performances compared to those of other similar programs.[37] The GoldScore-CS docking protocol was adopted in this study.[38] In this protocol, the poses obtained with the original GoldScore function were rescored and reranked with the GOLD implementation of the ChemScore function.[38,39]

was **S-1** whose enthalpic term was notably lower than that of **R-1**. This was in accordance with the crystal structures of the corresponding complexes of PPARγ with these two enantiomers, where the less active S-enantiomer realized less productive interactions with the protein because of a steric clash of its ethyl group with a residue of the helix 3.[25] The more disordered conformation of **S-1**, observed in the crystal structure, was also in accordance with the higher value of the entropic term obtained by ITC that partly compensated the low enthalpy value.

From Table 2, it is possible to observe, across the series, that the entropic term decreases by reducing the size of the substituents at the α position of the carboxylic group. This effect, known as "hydrophobic effect", was due to the decreasing buried surface of contact between the C-alpha substituents and the surface of the protein resulting in a less favorable entropic contribution.

**Table 2. Thermodynamic Parameters Relating to the Formation of the Complexes PPARγ-LBD/Ligand Determined by the ITC Assay**[a]

| ligand | $n$ | $K_d$ (μM) | $\Delta G$ (kcal/mol) | $\Delta H$ (kcal/mol) | $T\Delta S$ (kcal/mol) |
|---|---|---|---|---|---|
| R-1 | 0.92 ± 0.01 | 0.27 | −8.9 | −4.3 ± 0.07 | −4.6 |
| S-1 | 0.57 ± 0.07 | 2 | −7.8 | −1.1 ± 0.04 | −6.7 |
| 2 | 1.08 ± 0.04 | 4.5 | −7.3 | −4.1 ± 0.02 | −3.2 |
| R-3 | 0.22 ± 0.01 | 1.5 | −8.0 | −4.5 ± 0.19 | −3.5 |
| S-3 | 0.31 ± 0.01 | 3.3 | −7.5 | −5.8 ± 0.02 | −1.7 |
| 4 | 0.63 ± 0.03 | 7.7 | −7.0 | −5.7 ± 0.04 | −1.3 |
| rosiglitazone | 0.43 ± 0.01 | 0.12 | −9.4 | −5.0 ± 0[b] | −4.4 |

[a] $n$ = molar binding ratio of the ligand—protein interaction (observed stoichiometry). [b] This value was kept fixed during the fitting by Origin.

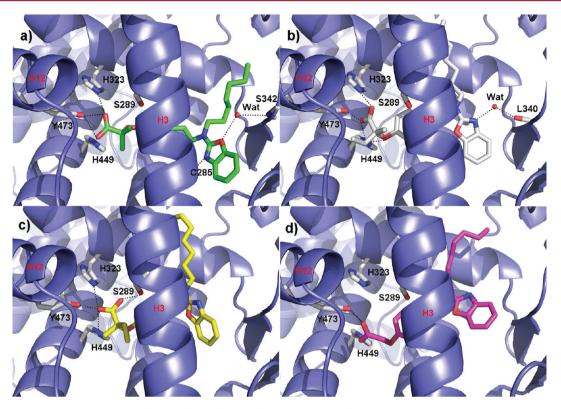**Figure 4.** H-bond network of compounds **2** (a, green), **R-1** (b, white), and **S-1** (c, yellow) in the crystal complex with PPARγ represented as a slate blue ribbon model. (d) Compound **4** (magenta) docked into the PPARγ binding site. Only amino acids involved in the H-bonding network with the ligand are displayed (white) and labeled. H-bonds discussed in the text are depicted as dashed black lines.

To test the validity of this protocol for the PPAR system, the crystallized conformation of ligand **2** was first docked back into its binding site. In this docking run, the 200 poses produced by GOLD resulted in only one prevailing cluster on the basis of their conformations: 43 of the poses closely resembled the crystallized conformation with a heavy atom root-mean-square deviation (rmsd) ranging from 0.9 to 2.3 Å. ChemScore was able to rank 25 out of the 43 poses from this cluster as the highest ranked 25 poses. Figure 1 of Supporting Information shows the comparison between the predicted docked conformation of **2** and the one observed in the crystal structure (rmsd = 1.91 Å). Thus, this docking protocol was considered to be suitable for the subsequent docking runs for compound **4**.

When **4** was docked within the PPARγ binding site, about 70% of the conformations generated by GOLD adopted only one highly conserved orientation lying in the same region occupied by **R-1**, **S-1**, and **2**. As can be seen in Figure 4d, ligand **4** loses the H-bond with both H323 and S289 side chains as its carboxylate group assumes a different conformation with respect to **2**, **R-1**, and **S-1**. Moreover, the long aliphatic chain and the benzoxazole ring of the ligand occupy the upper and lower parts of the distal cavity, respectively, there making hydrophobic contacts with the surrounding protein residues. In particular, the benzoxazole moiety of the ligand contacts the side chain of I341 belonging to the β-sheet.

As reported in Table 1, the potency of **2** is higher than that of both **S-1** and **4** on the same receptor. This behavior can be interpreted at the molecular level by the more efficient H-bonding network realized by the carboxylate of **2**, with particular regard to H12. A similar arrangement has been observed in the crystal complex of PPARγ with the more potent **R-1**[25] (Figure 4b). As shown in Figure 5, **R-1** and **2** interact in a
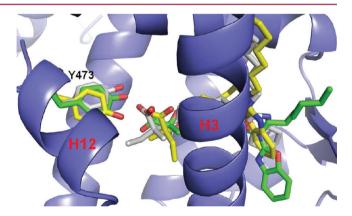


**Figure 5.** Superposition of the crystal structures of PPARγ in complex with **R-1** (white), **S-1** (yellow), and **2** (green).

similar way with Y473 of H12, while **S-1** forces the side-chain of the tyrosine to assume a different orientation, probably less efficacious for a good stabilization of this helix.[25] On the contrary, the less potent **S-1** and **4**, forming a less effective H-bonding network, weakly contribute to the H12 stabilization.

As far as the affinity is concerned, a good correlation with the potency can be observed in the case of the chiral compounds, where the R-enantiomers show higher affinity and potency with respect to the S-enantiomers. This correlation is not so evident for the achiral compounds **2** and **4**, where the higher potency, compared to that of other compounds of the series, could depend on the better stabilization of H12, as seen in the crystal structure of **2**. As a general rule, the affinity across the series is also driven by the "hydrophobic effect" which affects the entropic term. Moreover, our molecular modeling and X-ray studies show that the partial agonism of the ligands **S-1**, **2**, and

**4** toward PPARγ is in accordance with a better stabilization of H3 and/or the β-sheet, as discussed extensively in previous works.[25,26]

**Adipogenic and in Vivo Activities.** We first verified whether **R-1** and **S-1** were able to induce adipocyte differentiation of 3T3-L1 mouse fibroblasts, as PPARγ is a key determinant in this process. As shown in Figure 6A, both **R-1** and **S-1** increased the expression of PPARγ target genes like fatty acid binding protein 4 (Fabp4), the insulin sensitive glucose transporter (Glut4), and adiponectin (Acrp30), which are typically increased in differentiated adipocytes and represent adipose markers. Furthermore, we observed that these ligands induced lipid accumulation as a consequence of differentiation to adipocytes (Figure 6C). In particular, the quantitation of lipid content confirmed that cells differentiated in the presence of **R-1** or **S-1** and accumulated lipids to a level similar to that observed with the classical differentiation cocktail containing insulin, dexamethasone and IBMX or with the PPARγ full agonist rosiglitazone (Figure 6B).

Having ascertained that both **R-1** and **S-1** induced the adipogenic program in a PPARγ-dependent manner, we decided to explore the in vivo pharmacological properties by administering the two ligands to a mouse model of insulin resistance induced by the diet. Mice were fed a high fat diet for 16 weeks and then were treated with **R-1** (10 mg/kg/day), **S-1** (25 mg/kg/day), or the PPARγ agonist rosiglitazone (10 mg/kg/day) for 2 weeks. At the end of the treatment, the body weight of mice treated with **R-1** was significantly decreased (12% reduction) as compared to control mice (HFD) (Figure 7A). The body weight of mice on rosiglitazone was similar to that of HFD mice, while the decrease of body weight of mice treated with **S-1** (7% reduction) did not reach the statistical significance (Figure 7A). The analysis of fat deposits revealed that the visceral white adipose tissue (WAT) of mice administered with **R-1** or **S-1** was dramatically reduced as determined by magnetic resonance imaging (MRI), whereas rosiglitazone was not effective on this parameter (Figure 7B and C). In this respect, the decreased body weight observed with **R-1** and the reduced visceral fat obtained with both the R- and S-enantiomers represent an advantage versus rosiglitazone, whose administration is usually associated with increased adipogenesis and body weight in diabetic patients.[40] In a Gal4-based assay, we had previously shown that both **R-1** and **S-1** are dual PPARα/γ ligands;[25] therefore, to confirm their behavior as PPARα ligands we measured the expression of target genes in the liver of these mice and found that the mRNA levels of the mitochondrial medium-chain acyl-CoA dehydrogenase (Acadm), long-chain acyl-CoA dehydrogenase (Acadl), and of the peroxisomal acyl-Coenzyme A oxidase 1 (Acox1) were significantly increased by both enantiomers (Figure 2A of Supporting Information). In parallel, the liver weight of mice treated with **R-1** and **S-1** rose as compared to that of the control mice (Figure 2B of Supporting Information). This effect is typically observed in rodents treated with fibrates and PPARα agonists as confirmed in the group of mice on fenofibrate (Figure 2B of Supporting Information).[41,42]

High body weight and increased content of visceral fat have been recognized as risk factors for insulin resistance.[43,44] The improvement of morphometric parameters and the decreased visceral fat observed in mice treated with the two enantiomers suggest that the metabolic profile of these mice could have benefited from the administration of **R-1** or **S-1**. In fact, the levels of circulating triglycerides, nonesterified fatty acids

(NEFA), glucose, and insulin were reduced with both **R-1** and **S-1** (Figure 8). Cholesterol levels were not affected by any of the tested ligands (data not shown). The changes of the metabolic profile elicited by the two enantiomers indicated that these ligands might be insulin sensitizers in vivo. To test this hypothesis, we carried out the oral glucose tolerance test and the insulin tolerance test, two standard assays widely used to assess insulin resistance and basal insulin sensitivity by following the evolution of glucose levels after a glucose load or insulin injection, respectively.[45] We found that mice on **R-1** were able to improve the glucose clearance upon an oral load as compared to control (HFD) mice (Figure 9A and inset). Conversely, the glucose clearance following the oral load in mice on **S-1** was slightly improved but did not reach the statistical significance (Figure 9A and inset). Similarly, the insulin-induced increase in glucose disposal rate was significantly higher in mice treated with **R-1**, suggesting increased insulin sensitivity in this group of mice, while the curve with the S-enantiomer was improved, but the difference with the control group was not statistically significant (Figure 9B and inset). It should be mentioned, however, that **S-1**, although to a lesser extent than **R-1**, reduced the circulating levels of glucose and insulin in fasted mice, reflecting the beneficial outcome of PPARγ stimulation in vivo with the S-enantiomer. In fact, the calculation of the homeostatic model assessment of insulin resistance (HOMA-IR), an index of insulin resistance, shows that **R-1** and **S-1** decreased insulin resistance (Figure 9C) consistent with the reduced plasma levels of glucose and insulin achieved with these two PPARγ ligands (Figure 8). Notably, by using a combination of structural studies with techniques to examine the selective coregulator recruitment, we have recently shown that **S-1** is a partial agonist of PPARγ able to recruit a different set of coregulators as compared to the R-enantiomer.[26] On the basis of these molecular approaches, we proposed that this ligand may be a SPPARγM. Yet, since **S-1**, as well as **R-1**, also activates PPARα, it is likely that the pharmacological profile obtained with these two ligands may arise from the combined action on these two receptor subtypes. It should be mentioned that, unlike selective PPARγ agonists, it is well-known that dual PPARα/γ agonists do not show weight gain in rodent models of diabetes.[46] It will be interesting in the future to test in cell and animal models whether **S-1** is able to uncouple the improved metabolic profile from the side effects usually observed in patients treated with thiazolidinediones.[47]

**Effects on Cell Proliferation.** Next step in this study was to evaluate the antitumor effects of **R-1** and **S-1** in colon cancer cell lines. We chose these compounds with the aim of examining if there was difference, with regard to this type of activity, between full and a partial PPARγ agonists. In fact, clinical trials on the full agonists TZDs as antineoplastic agents have shown, so far, conflicting results, justifying the need to further investigate the anticancer potential of PPARγ agonists.[48]

The first step was the Western blot analysis of PPARγ expression in our in vitro panel. The three cell lines utilized in this study (HT-29, LoVo, and HCT15) showed highly expressed PPARγ. This expression profile was in support of the use of these cells for our study and confirmed the existence of the PPARγ signaling system in such malignant cells (Figure 10). The capability of **R-1** and **S-1** to inhibit tumor cell growth was analyzed using the full PPARγ agonist troglitazone as a reference compound. All cell lines were incubated for 1 and 2 days with each compound at various
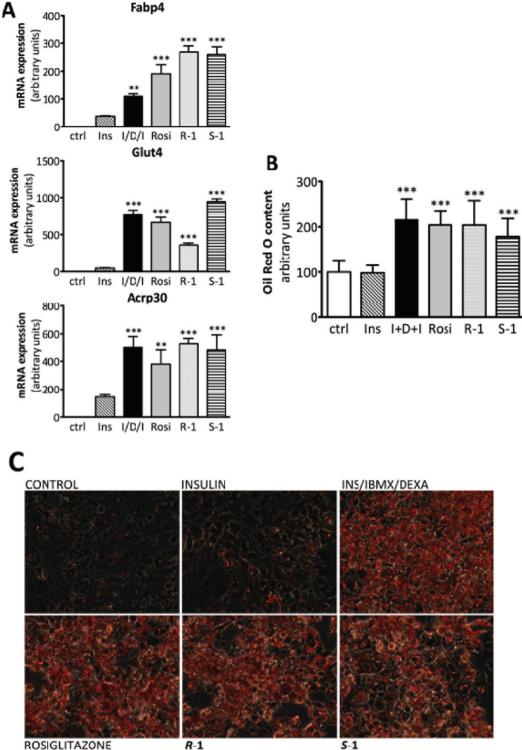
**Figure 6.** Expression of PPARγ target genes and lipid accumulation in murine adipocytes. (Panel A) 3T3-L1 mouse fibroblasts were differentiated in the presence of the indicated treatments. Total RNA was extracted, and the expression of Fabp4, Glut4 and Acrp30 was measured by real time qPCR. ctrl, control samples; Ins, samples treated with 5 μg insulin·mL$^{-1}$; I/D/I, samples treated with 10 μg insulin·mL$^{-1}$, 1 μM dexamethasone, and 0.5 mM IBMX; Rosi, 1 μM rosiglitazone; **R-1**, 1 μM **R-1**; **S-1**, 1 μM **S-1**. Data are expressed as the mean ± SD of triplicate samples. (Panel B) Spectrophotometric quantification of lipid content after solvent extraction of Oil Red O from mouse adipocytes differentiated in the presence of the indicated treatments. Results are expressed as the mean ± SD ($n = 4$). (**) and (***) indicate statistical significance at $p < 0.01$ and $p < 0.001$, respectively. (Panel C) 3T3-L1 mouse fibroblasts were differentiated to adipocytes in the presence of the indicated treatments. Cells were stained with Oil Red O, and pictures were taken with an Axiovert 200 microscope at 20× magnification.

concentrations (range 1−100 μM); the cell growth inhibition was analyzed by the MTT assay, and the IC$_{50}$ was determined. A cell proliferation inhibition in dose- and time-dependent manner was observed. After one day of drug exposure, a cell growth inhibition was obtained with IC$_{50}$ higher than 100 μM (data not shown). The inhibitory effects were significantly
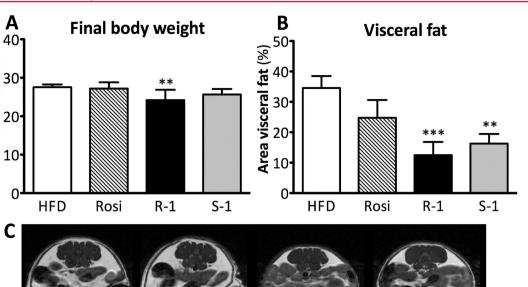
**Figure 7.** Effect of PPARγ ligands on body weight and visceral fat content in HFD fed mice. Six weeks old C57Bl/6J male mice were fed a high fat diet for 16 weeks and subsequently were treated with the indicated ligands for two weeks as detailed in the Experimental Section. (Panel A) Body weight of mice at the end of the treatments (6 mice/treatment group). (Panel B) Quantification of visceral fat by MRI of total body fat; results are expressed as the percentage of visceral fat area on the total image (the MRI analysis was performed on 3 mice/treatment group). (Panel C) representative image of MRI performed on mice treated with the indicated ligands. (**) and (***) indicate statistical significance at $p < 0.01$ and $p < 0.001$, respectively.
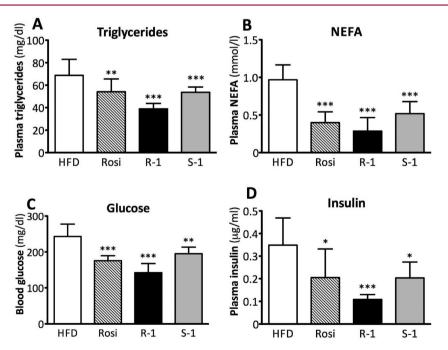


**Figure 8.** Plasma levels of glucose, lipids, and hormones in HFD mice treated with PPARγ ligands. The quantification of plasma levels of triglycerides (panel A), NEFA (panel B), glucose (panel C), and insulin (panel D) was performed on the same mice described in Figure 7 treated with the indicated ligands. (*), (**), and (***) indicate statistical significance at $p < 0.05$, $p < 0.01$, and $p < 0.001$, respectively.

increased when cells were treated for 2 days; in this case, in all cell lines IC$_{50}$ ranged between 17 and 65 μM with **R-1** and **S-1**, which were more potent than troglitazone on LoVo and HCT15 cells. As shown in Table 3, however, no significantly different antiproliferative activity was observed between the two enantiomers.

To investigate if the cell growth inhibition occurred through PPARγ activation, tumor cell lines were incubated for 48 h with each of the enantiomers (IC$_{50}$) and/or the potent PPARγ antagonist **6** (GW9662)[49] (20 μM). Compound **6** is itself an inhibitor of cell proliferation, but it acts by a PPARγ-independent mechanism.[50] Cell viability was analyzed by the MTT assay, and in two of the investigated cell lines, **6** neither inhibited cell proliferation nor reversed growth inhibition induced by **R-1** and **S-1** (data not shown); our ligands, in fact, still induced cell growth suppression, even though PPARγ was blocked. In such experimental conditions, only HT-29
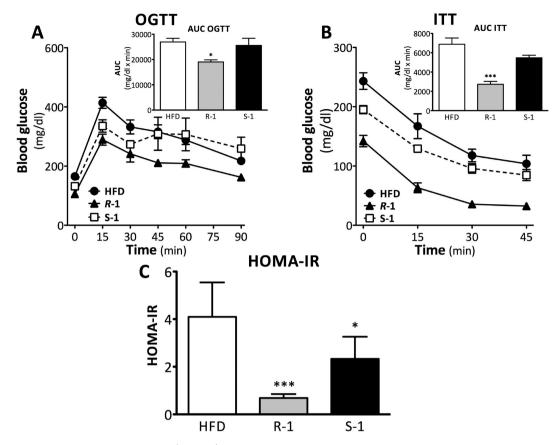
**Figure 9.** R-enantiomer is an insulin sensitizer. (Panel A) Four days before sacrifice, HFD mice treated as indicated in the figure were fasted overnight and underwent an oral glucose tolerance test. Results are expressed as the mean ± SE of plasma glucose levels at the indicated time points in at least five animals/group. Area under the curves (AUC) were calculated and plotted (inset). (Panel B) Two days before sacrifice, HFD mice treated as indicated in the figure were fasted for 6 h and underwent an insulin tolerance test. Results are expressed as the mean ± SE of plasma glucose levels at the indicated time points in at least five animals/group. Area under the curves (AUC) were calculated and plotted (inset). (Panel C) HOMA-IR index was calculated for the indicated treatments. Results are expressed as the mean ± SD of at least five animals/group. (*) and (***) indicate statistical significance at $p < 0.05$ and $p < 0.001$, respectively.
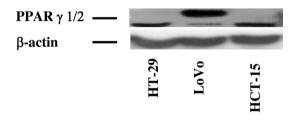


**Figure 10.** PPARγ expression. Protein extracts from LoVo, HT-29, and HCT-15 cells were analyzed by Western blot to analyze the expression level of PPARγ. β-Actin expression level was used to normalize the sample value.

**Table 3. Effectiveness of R-1, S-1, and Troglitazone in Colon Tumour Cell Lines**

| compd | IC$_{50}$ (µM) | | |
|---|---|---|---|
| | HTC-15 | HT-29 | LoVo |
| S-1 | 21 ± 1.2 | 50 ± 3.1 | 17 ± 3.2 |
| R-1 | 17 ± 1.6 | 41 ± 3.5 | 19 ± 2.3 |
| troglitazone | 50.9 ± 1.6 | 50 ± 2.8 | 65 ± 4.8 |

cells showed about 40% loss of viability in response to **6**. Co-treatment of these cells with each of the enantiomers and **6**, instead, resulted in a recovery of proliferation, and this effect was much more evident when **6** was added to **R-1** than to **S-1**

(Figure 11A). This data suggests the direct involvement of PPARγ in mediating the antiproliferative activity of *R-1* and *S-1* in HT-29 cells. In the case of *R-1*, however, the complete recovery of proliferation allows one to hypothesize a simultaneous interference from *R-1* and, partially, *S-1* in the pathway responsible for the cytotoxicity of **6**, which, as already mentioned, acts by a PPARγ-independent mechanism. This could explain why, under cotreatment conditions, **6** did not exhibit any growth inhibition. Further investigations in this field are in progress.

To evaluate which phase all the cell lines investigated were blocked in, we examined the cell cycle by flow cytometry analysis. Compared to control cells, an increase of the G0/G1 phase was observed, as shown in Figure 11B for HT-29, after treatment with *R-1* and *S-1*, at different times, suggesting that our ligands reduced tumor cell growth via G0/G1 cell arrest. Next, we verified if the G0/G1 block in HT-29 was mediated by PPARγ activation. Flow cytometry of cell cycle revealed that the activity of *R-1* and *S-1* on HT-29 was altered when these cells were simultaneously treated with the PPARγ antagonist **6**. In particular, the G0/G1 block induced by *S-1*, which appeared after 2 days of treatment, was resumed by **6**. Differently, *R-1* blocked the cells already after 1 day, and this block was persistent after 48 h. In this case, the presence of **6** allowed the cells to recover the baseline rate of cell cycle progression after 1 day, whereas no response to **6** was observed after 2 days
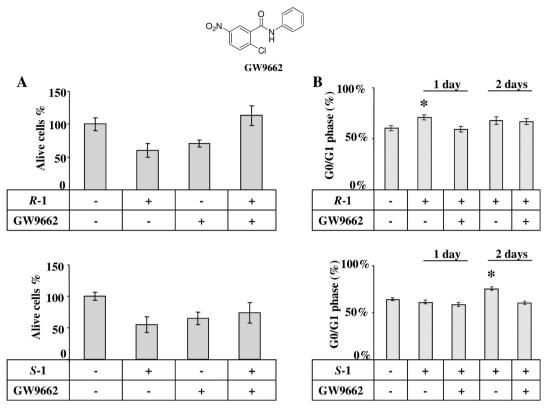
**Figure 11.** (Panel A) PPARγ activation involvement in cell growth inhibition by **R-1** and **S-1**. HT-29 cells were incubated, for two days, with each of the enantiomers ($IC_{50}$) and/or **6** (20 μM), and the cell growth modulation was analyzed by MTT assay as described in the Experimental Section. (Panel B) Cell cycle modulation. HT-29 cells were incubated, for one and two days, with each of the enantiomers **R-1** and **S-1** ($IC_{50}$) and/or **6** (20 μM), and the cell cycle was analyzed by flow cytometry. The reported G0/G1 phase percentages are the means of three different experiments ± SD. Significance of the differences was $p < 0.05$ (*).

under the same conditions suggesting that this effect could be only partially related to PPARγ activation in this cell line (Figure 11B).

Finally, we evaluated if **R-1** and **S-1** could effectively induce apoptosis in the HT-29 cell line. For this purpose, these cancer cells were treated with both enantiomers and troglitazone for 24 and 48 h at the corresponding $IC_{50}$ concentrations. Fluorescein isothiocyanate-conjugated annexin V was utilized to detect the externalization of phosphatidylserine that occurs at an early stage of apoptosis. Propidium iodide was used as a marker of necrosis due to cell membrane destruction. As shown in Figure 12, all the compounds effectively induced apoptosis in a time-dependent manner.

## ■ CONCLUSIONS

A short series of ureidofibrate-like derivatives endowed with PPARγ activity was prepared by modifying the substituents at α position of the carboxylic group. The use of calorimetric techniques (DSC, ITC) turned out to be a valuable approach for the determination of the thermodynamic parameters associated with the formation of the receptor−ligand complexes. The behavior of some compounds of the series was rationalized by performing docking experiments and X-ray studies which provided a molecular explanation for their different potency and efficacy. Different aspects of the biological activity of the full and partial agonists **R-1** and **S-1**, respectively, were also evaluated. On the basis of the results obtained in cultured adipocytes and in HFD mice, we conclude that the two enantiomers activate PPARγ target genes and have
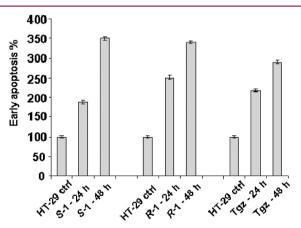


**Figure 12.** Apoptotic effect of **S-1** and **R-1**. HT-29 cells were treated for 2 days with **S-1** or **R-1** or troglitazone at the corresponding $IC_{50}$ concentration. Apoptosis detection was performed by Annexin V-FITC staining assays and propidium iodide (PI), in accordance with the manufacturer's instructions followed by FACS analysis. The histogram represents the mean ± SEM of apoptosis rates obtained from three independent experiments.

profound effects on the metabolic profile in vivo. These ligands also activate PPARα in the liver, and this is likely to contribute to their pharmacological profile. The two enantiomers improved morphometric and metabolic parameters and reduced insulin resistance most likely as a consequence of decreased body weight and visceral fat, which are usually associated with insulin resistance and type 2 diabetes.[43,44] Furthermore, our data obtained in different colon cancer cell

lines indicate that these two stereoisomers not only potently inhibit cell growth, even though by a mechanism of action only partially related to PPARγ activation, but also effectively induce apoptosis in cancer cells. Collectively, the results of this preliminary integrated study allow one to claim that **R-1** and **S-1** represent dual PPARα/γ ligands with promising biological effects in cellular systems and in an animal model of insulin resistance and could stand, therefore, as leads for the development of new molecules for the treatment of type 2 diabetes and/or cancer.

### ■ EXPERIMENTAL SECTION

**Chemical Methods.** Column chromatography was performed on ICN silica gel 60 Å (63−200 μm) as a stationary phase. Melting points were determined in open capillaries on a Gallenkamp electrothermal apparatus and are uncorrected. Mass spectra were recorded with a HP GC/MS 6890-5973 MSD spectrometer, electron impact 70 eV, equipped with HP chemstation. For GC/MS analysis of acid analytes, the corresponding methyl esters, obtained by reaction with a solution of diazomethane in $Et_2O$, were used. $^1$H NMR spectra were recorded in $CDCl_3$ on a Varian-Mercury 300 (300 MHz) spectrometer at room temperature (20 °C). Chemical shifts are expressed as parts per million ($\delta$). The purity of all tested compounds was >95%, as confirmed by combustion analysis carried out with an Eurovector Euro EA 3000 model analyzer. Optical rotations were measured with a Perkin-Elmer 341 polarimeter at room temperature (20 °C): concentrations are expressed as g(100 mL)$^{-1}$. The enantiomeric excesses of the final acids were determined by HPLC analysis on Chiralcel OD column (4.6 mm i.d. × 250 mm, Daicel Chemical Industries, Ltd., Tokyo, Japan). Analytical liquid chromatography was performed on a PE chromatograph equipped with a Rheodyne 7725i model injector, a 785A model UV/vis detector, a series 200 model pump, and an NCI 900 model interface. Chemicals were obtained from Aldrich (Milan, Italy), Lancaster (Milan, Italy), or Acros (Milan, Italy) and were used without any further purification.

**Preparation of Methyl or Ethyl 2-[4-(2-Heptanoylamino-ethyl)phenoxy]-α-substituted-ethanoate (2b−5b).** Heptanoic acid (9.00 mmol), HOBT·$x$H$_2$O (3.00 mmol), and DIC (11.25 mmol) were added to a solution of the appropriate compound **2a−5a** (6.00 mmol) in CH$_2$Cl$_2$ (50 mL). The reaction mixture was stirred for 15 h at room temperature. The organic phase was washed with NaHCO$_3$ saturated solution, 1 N HCl, and brine, then dried over Na$_2$SO$_4$, and filtered. The solvent was evaporated to dryness affording a yellow solid residue which was chromatographed on a silica gel column (petroleum ether/ethyl acetate from 8:2 to 3:7 as eluents) to give the desired compounds in 70−89% yields.

*Methyl 2-[4-(2-Heptanoylamino-ethyl)phenoxy]-2-methyl-propanoate (**2b**).* Yellow oil, 89% yield.

*S-Methyl 2-[4-(2-Heptanoylamino-ethyl)phenoxy]propanoate (**S-3b**).* White solid, 71% yield.

*R-Methyl 2-[4-(2-Heptanoylamino-ethyl)phenoxy]propanoate (**R-3b**).* White solid, 73% yield.

*Ethyl 2-[4-(2-Heptanoylamino-ethyl)phenoxy]ethanoate (**4b**).* Yellow oil, 86% yield.

*S-Methyl 2-[4-(2-Heptanoylamino-ethyl)phenoxy]-3-phenyl-propanoate (**S-5b**).* White solid, 70% yield.

*R-Methyl 2-[4-(2-Heptanoylamino-ethyl)phenoxy]-3-phenyl-propanoate (**R-5b**).* White solid, 71% yield.

**Preparation of Methyl or Ethyl 2-[4-(2-Heptylamino-ethyl)-phenoxy]-α-substituted-ethanoate.** One molar BH$_3$ in THF solution (10 mmol) was added, under N$_2$ atmosphere, to a stirred solution of the appropriate compound **2b−5b** (1.22 mmol) in anhydrous THF (15 mL). The reaction mixture was stirred overnight at room temperature, then was carefully added with MeOH (15 mL), and stirred for 0.5 h at reflux. The organic solvent was evaporated to give a colorless oily residue in quantitative yield, which was used for the next step without any further purification.

**Preparation of Methyl or Ethyl 2-{4-[2-(N-Heptyl-N-(benzox-azol-2-yl)amino-ethyl)]phenoxy}-α-substituted-ethanoate**

**(2c−5c).** The appropriate amine intermediate was dissolved in THF (15 mL), cooled to 0 °C, and added with N(Et)$_3$ (0.2 mL) and a solution of 2-chlorobenzoxazole (2.20 mmol) in anhydrous THF (5 mL). The resulting reaction mixture was stirred for 0.5 h at 0 °C, 0.5 h at room temperature, 2 h at reflux, and 15 h at room temperature. The organic solvent was evaporated to dryness affording a solid residue which was chromatographed on a silica gel column (petroleum ether/ethyl acetate 9:1 as eluent) to give the title compounds in 42−71% yield.

*Methyl 2-{4-[2-(N-Heptyl-N-(benzoxazol-2-yl)amino-ethyl)]-phenoxy}-2-methyl-propanoate (**2c**).* Colorless oil, 71% yield.

*S-Methyl 2-{4-[2-(N-Heptyl-N-(benzoxazol-2-yl)amino-ethyl)]-phenoxy}propanoate (**S-3c**).* Colorless oil, 45% yield.

*R-Methyl 2-{4-[2-(N-Heptyl-N-(benzoxazol-2-yl)amino-ethyl)]-phenoxy}propanoate (**R-3c**).* Colorless oil, 42% yield.

*Ethyl 2-{4-[2-(N-Heptyl-N-(benzoxazol-2-yl)amino-ethyl)]-phenoxy}ethanoate (**4c**).* Yellow oil, 47% yield.

*S-Methyl 2-{4-[2-(N-Heptyl-N-(benzoxazol-2-yl)amino-ethyl)]-phenoxy}-3-phenyl-propanoate (**S-5c**).* Colorless oil, 66% yield.

*R-Methyl 2-{4-[2-(N-Heptyl-N-(benzoxazol-2-yl)amino-ethyl)]-phenoxy}-3-phenyl-propanoate (**R-5c**).* Colorless oil, 61% yield.

**Preparation of the Final Compounds 2−5.** A solution of the corresponding alkyl ester **2c−5c** (0.85 mmol), obtained from the previous steps, in EtOH (10 mL) and 1 N NaOH (5 mL) was stirred for 5 h at room temperature. The organic solvent was removed under reduced pressure and the aqueous phase was acidified with 2 N HCl and extracted with ethyl acetate. The organic layer was dried over Na$_2$SO$_4$, filtered, and evaporated to dryness affording the title compounds in quantitative yields as a white solid (**2**) or colorless oils (**4**, both enantiomers of **3** and **5**). The oily acids were transformed into the corresponding sodium (**R-3**, **S-3**, and **4**) or cyclohexylamine salts (**R-5** and **S-5**). For this purpose, to a solution of the appropriate acid (1.5 mmol) in 95% EtOH (20 mL) was added NaHCO$_3$ (1.5 mmol) or cyclohexylamine (2.0 mmol). The reaction mixture was stirred overnight at rt. The solvent was evaporated to dryness to give the desired salts as white solids, which were recrystallized by the suitable solvent.

*2-{4-[2-(N-Heptyl-N-(benzoxazol-2-yl)amino-ethyl)]phenoxy}-2-methyl-propanoic Acid (**2**).* White solid, 52% yield (CHCl$_3$/$n$-hexane).

*(−)-S-Sodium 2-{4-[2-(N-Heptyl-N-(benzoxazol-2-yl)amino-ethyl)]phenoxy}propanoate (**S-3**).* White solid, 45% yield (CHCl$_3$/$n$-hexane).

*(+)-R-Sodium 2-{4-[2-(N-Heptyl-N-(benzoxazol-2-yl)amino-ethyl)]phenoxy}propanoate (**R-3**).* White solid, 49% yield (CHCl$_3$/hexane).

*Sodium 2-{4-[2-(N-Heptyl-N-(benzoxazol-2-yl)amino-ethyl)]-phenoxy}ethanoate (**4**).* White solid, 34% yield (CHCl$_3$/$n$-hexane).

*(−)-S-Cyclohexylammonium 2-{4-[2-(N-Heptyl-N-(benzoxazol-2-yl)amino-ethyl)]phenoxy}-3-phenyl-propanoate (**S-5**).* White solid, 29% yield (AcOEt/CHCl$_3$).

*(+)-R-Cyclohexylammonium 2-{4-[2-(N-Heptyl-N-(benzoxazol-2-yl)amino-ethyl)]phenoxy}-3-phenyl-propanoate (**R-5**).* White solid, 70% yield (AcOEt/CHCl$_3$).

**Preparation of Methyl 2-(4-Bromo-phenoxy)-2-methyl-propanoate (2d).** A solution of KOH (2.92 g, 5.21 mmol) in H$_2$O (10 mL) was added dropwise to a solution of 4-bromo-phenol (1.51 g, 8.68 mmol) in acetone (15 mL). After 0.5 h at room temperature, a first amount of CHBr$_3$ (0.60 mL) was added dropwise, during 10 min, to the reaction mixture. After 1 h at room temperature, a second addition of CHBr$_3$ (1.2 mL) was carried out, during 15 min. The resulting mixture was stirred overnight at room temperature after which the organic solvent was distilled off. The aqueous phase was carefully acidified with 6 N HCl and extracted with ethyl acetate. The collected organic phase was washed with brine, dried over Na$_2$SO$_4$, filtered, and evaporated to dryness affording a brown oily residue, which was dissolved in ethyl acetate and extracted five times with NaHCO$_3$ saturated solution. The aqueous phase was carefully acidified with 6 N HCl and extracted four times with Et$_2$O. The collected organic layer was dried over Na$_2$SO$_4$, filtered, and evaporated to dryness to give a dark red oily residue, which was chromatographed on a silica gel column (petroleum ether/ethyl acetate/MeOH 7:2:1 as

eluent) affording the desired acid as a pale yellow solid in 70% yield. A solution of this acid (5 mmol) in MeOH (20 mL) and two drops of concd $H_2SO_4$, was stirred for 3 h at reflux, then the solvent was distilled off, and the residue was dissolved in ethyl acetate. The resulting solution was washed with $NaHCO_3$ saturated solution and brine, then the organic phase was dried over $Na_2SO_4$, and the solvent was removed under reduced pressure to give the title compound as a pale yellow oil in quantitative yield.

**Preparation of *S*- or *R*-Methyl 2-(4-bromo-phenoxy)-3-phenyl-propanoate (5d).** A solution of diisopropylazodicarboxylate (DIAD, 2.81 g, 13.90 mmol) in anhydrous toluene (20 mL) was added dropwise to an ice-bath cooled mixture of *R*- or *S*-methyl phenyllactate (2.51 g, 13.87 mmol), 4-bromophenol (2.45 g, 13.89 mmol), and triphenylphosphine (3.64 g, 13.88 mmol) in anhydrous toluene (50 mL). The reaction mixture was stirred at room temperature overnight, under $N_2$ atmosphere. Toluene was evaporated in vacuo, and a mixture of $Et_2O$ and hexane (50 mL, 1:1) was added to the residue. The resulting precipitate was filtered off, and the filtrate was evaporated to dryness. The residue was chromatographed on a silica gel column (petroleum ether/ethyl acetate 9:1 as eluent) affording the desired compound as a colorless oil in 76% yields.

**Preparation of Methyl 2-[4-(2-Phthalimido-2-yl-ethen)-phenoxy]-2-methyl- or 3-Phenyl-propanoate.** A solution of **2d** or *S*- or *R*-**5d** (6.0 mmol), tri-*o*-tolylphosphine (0.50 mmol), *N*-vinyl-phthalimide (6.0 mmol), and *N,N*-diisopropylethylamine (9.5 mmol) in anhydrous $CH_3CN$ (15 mL) was added, under $N_2$ atmosphere, to a suspension of $Pd(AcO)_2$ (0.20 mmol) in the same anhydrous solvent (3 mL). The reaction mixture was stirred for 24 h at reflux, then the organic solvent was evaporated in vacuo, and $CH_2Cl_2$ (20 mL) was added to the residue. The precipitate was filtered off through a Celite pad, washed four times with $CH_2Cl_2$ (20 mL), and the filtrate was washed with brine and dried over $Na_2SO_4$. The solvent was evaporated to dryness affording a yellow solid residue, which was chromatographed on a silica gel column (petroleum ether/ethyl acetate 9:1 as eluent) to give the title compound as a yellow solid, in 75−89% yield, which was used in the next step without any further purification.

*Methyl 2-[4-(2-Phthalimido-2-yl-ethen)phenoxy]-2-methyl-propanoate.* 89% yield.

*S-Methyl 2-[4-(2-Phthalimido-2-yl-ethen)phenoxy]-3-phenyl-propanoate.* 87% yield.

*R-Methyl 2-[4-(2-Phthalimido-2-yl-ethen)phenoxy]-3-phenyl-propanoate.* 75% yield.

**Preparation of Methyl 2-[4-(2-Phthalimido-2-yl-ethyl)-phenoxy]-2-methyl or 3-Phenyl-propanoate (2e, *S*- and *R*-5e).** A solution of the intermediate obtained in the previous step (6.0 mmol) in THF (35 mL) was added to a stirred suspension of Wilkinson catalyst (0.40 mmol) in abs EtOH (5 mL). The resulting mixture was stirred at room temperature under $H_2$ atmosphere (4 atm) for 5 h. The suspension was filtered through a Celite pad to remove the catalyst, and the solvent was evaporated to dryness providing a dark solid residue which was chromatographed on a silica gel column (petroleum ether/ethyl acetate 7:3 as eluent), affording the desired compounds as a yellow solids in 70−87% yield.

*Methyl 2-[4-(2-Phthalimido-2-yl-ethyl)phenoxy]-2-methyl-propanoate (2e).* 70% yield.

*S-Methyl 2-[4-(2-Phthalimido-2-yl-ethyl)phenoxy]-3-phenyl-propanoate (S-5e).* 87% yield.

*R-Methyl 2-[4-(2-Phthalimido-2-yl-ethyl)phenoxy]-3-phenyl-propanoate (R-5e).* 85% yield.

**Preparation of Intermediates 2a and Both Enantiomers of 5a.** $N_2H_4 \cdot xH_2O$ (32 mmol) was added to a solution of **2e** or *S*- or *R*-**5e** (5.25 mmol) in absolute EtOH (40 mL). The reaction mixture was stirred for 1 h at reflux and overnight at rt. The suspension was filtered, and the organic solvent was evaporated in vacuo to give a yellow solid which was dissolved in ethyl acetate. The solution was washed with brine, dried over $Na_2SO_4$, and the organic solvent evaporated to dryness affording the desired compounds in 73−86% yield as yellow oils. The resulting amines were used in the next step without any further purification.

*Methyl 2-[4-(2-Amino-ethyl)phenoxy]-2-methyl-propanoate (2a).* 86% yield.

*S- and R-Methyl 2-[4-(2-Amino-ethyl)phenoxy]-3-phenyl-propanoate (5a).* 73% and 79% yields, respectively.

**Preparation of Benzyl 4-Hydroxy-phenetyl-carbamate.** $K_2CO_3$ (23.88 g, 172.8 mmol) and benzylchloroformate (8.2 mL, d = 1.195 g·mL$^{-1}$, 57.6 mmol) were added to a suspension of tiramine hydrochloride (10.0 g, 57.6 mmol) in $H_2O$ (310 mL) and $Et_2O$ (250 mL). The resulting mixture was stirred at room temperature for 4 h. The organic solvent was separated, washed with brine, dried over $Na_2SO_4$, and evaporated to dryness providing the desired compound as a white solid in 94% yield.

**Preparation of Intermediates *S*- and *R*-3d.** A solution of diisopropylazodicarboxylate (DIAD, 3.72 g, 18.42 mmol) in anhydrous THF (30 mL) was added dropwise to an ice-bath cooled mixture of *R*- or *S*-methyl lactate (1.96 g, 18.41 mmol), benzyl 4-hydroxy-phenetyl-carbamate (4.31 g, 18.40 mmol), and triphenylphosphine (4.84 g, 18.40 mmol) in anhydrous THF (30 mL). The reaction mixture was stirred at room temperature for 48 h, under $N_2$ atmosphere. THF was evaporated in vacuo, and a mixture of $Et_2O$ and hexane (50 mL, 1:1) was added to the residue. The resulting precipitate was filtered off, and the filtrate was evaporated to dryness. The residue was chromatographed on a silica gel column ($CHCl_3$/ethyl acetate 98:2 as eluent) affording the desired compounds as yellow oils in 50 and 57% yields, respectively.

**Preparation of 4d.** The benzyl 4-hydroxy-phenetyl-carbamate (4.01 g, 14.74 mmol) was added to an ice-bath cooled suspension of 95% NaH (1.13 g, 45.83 mmol) in anhydrous DMF (80 mL). The resulting mixture was stirred at 0 °C for 0.5 h, under $N_2$ atmosphere, and then was added dropwise with a solution of ethyl 2-bromoacetate (3.69 g, 22.16 mmol) in anhydrous DMF (20 mL). The reaction mixture was stirred at room temperature for 24 h, under $N_2$ atmosphere. The organic solvent was evaporated in vacuo, and the residue was dissolved in ethyl acetate. The solution was washed with ammonium chloride saturated solution, 0.5 N NaOH, and brine, then was dried over $Na_2SO_4$, and the organic solvent was evaporated to dryness affording the desired compound as a white solid in 95% yield.

**Preparation of Intermediates *S*- and *R*-3a and 4a.** Ten percent Pd/C (0.1 mmol) was added to a solution of the appropriate intermediate *S*-, *R*-3d, or 4d, (7.50 mmol) in abs. EtOH (100 mL). The resulting mixture was stirred at room temperature under $H_2$ atmosphere (5 atm) for 1.5 h. The suspension was filtered through a Celite pad to remove the catalyst, and the solvent was evaporated to dryness providing the desired compounds as oils in quantitative yields.

**PPAR Activity.** Reference compounds, medium, and other cell culture reagents were purchased from Sigma-Aldrich (Milan, Italy).

*Plasmids.* The expression vectors expressing the chimeric receptor containing the yeast Gal4-DNA binding domain fused to the human PPARα, PPARγ, or PPARβ/δ ligand binding domain (LBD), and the reporter plasmid for these Gal4 chimeric receptors (pGal5TKpGL3) containing five repeats of the Gal4 response elements upstream of a minimal thymidine kinase promoter that is adjacent to the luciferase gene were described previously.[51]

*Cell Culture and Transfections.* Human hepatoblastoma cell line HepG2 (for PPARα and PPARγ) or monkey kidney cell line COS-1 (for PPARβ/δ) (Interlab Cell Line Collection, Genoa, Italy) were cultured in Minimum Essential Medium (MEM, HepG2) or Dulbecco's Modified Eagle's Medium (DMEM, COS-1) containing 10% of heat-inactivated fetal bovine serum, 100 U penicillin G·mL$^{-1}$, and 100 μg streptomycin sulfate·mL$^{-1}$ at 37 °C in a humidified atmosphere of 5% $CO_2$. For transactivation assays, $10^5$ cells per well were seeded in a 24-well plate and transfections were performed after 24 h with CAPHOS (Sigma, Milan, Italy), a calcium-phosphate method, according to the manufacturer's guidelines. Cells were transfected with expression plasmids encoding the fusion protein Gal4-PPARα LBD or Gal4-PPARγ LBD or Gal4-PPARβ/δ LBD (30 ng), pGal5TKpGL3 (100 ng), and pCMVβgal (250 ng). Four hours after transfection, cells were treated for 20 h with the indicated ligands in triplicate. Luciferase activity in cell extracts was then determined by a luminometer (VICTOR$^3$ V Multilabel Plate Reader, PerkinElmer). β-Galactosidase activity was determined using β-D-galactopyranoside (Sigma, Milan, Italy) as described previously.[52] All transfection experiments were repeated at least twice.

**Differential Scanning Calorimetry.** DSC experiments were performed with a MicroCal VP-DSC microcalorimeter (MicroCal Inc., Northampton, MA, USA). The samples were dialyzed against the Hepes buffer (Hepes 20 mM, pH 8.0, TCEP 1 mM) and gently degassed before scanning. The LBD of PPARγ was expressed as the N-terminal His-tagged protein using a pET28 vector and purified as previously described.[25] The protein concentration was 10 $\mu$M, and the ligand concentration was 20 $\mu$M. The concentration of PPARγ (30.58 kDa) was determined spectrophotometrically using the extinction coefficient $E^{0.1\%}$ = 0.341 at 280 nm. The reference cell was filled with the same solvent mixture as that used for the sample, but lacking the protein. The experiment was performed ranging from 10 to 100 °C, and the heating rate was 1 °C·min$^{-1}$. Thermograms were corrected by subtracting the instrumental baseline, obtained with both cells filled with the same solvent, and normalized for protein concentration. When a post-transitional baseline could be determined, a progress baseline was subtracted; otherwise, a straight line connecting the initial and the final temperature of the overall transition was used.[53] $T_m$ (temperature of maximum heat capacity) and $\Delta H$ (heat reaction) were calculated using the Origin 7.0 software provided by MicroCal.

**Isothermal Titration Calorimetry.** ITC experiments were performed at 25 °C using a MicroCal ITC$_{200}$ microcalorimeter (MicroCal Inc., Northampton, MA, USA). PPARγ was extensively dialyzed against the buffer of choice (Hepes 20 mM, pH 8.0, TCEP 1 mM, or Tris-HCl 20 mM, pH 8.0, and TCEP 1 mM) with Amicon Ultra filters, and the final exchange buffer was then used to dilute the ligand stock solutions (20 or 50 mM in DMSO). DMSO was added to the protein solution at the same percentage of the ligand solution (below 5%). Samples were centrifuged before the experiments to eliminate possible aggregates. Protein and ligand solutions were degassed before use. Titrations were performed at 25 °C. The protein solution (30−120 $\mu$M) was placed in the sample cell, and the ligand solution (5−15 times more concentrated than the protein) was loaded into the syringe injector. The titrations involved 19 injections of 2 $\mu$L at 180 s intervals. The syringe stirring speed was set at 1000 rpm. Reference titrations of ligands into buffer were used to correct for heats of dilutions. Buffers of different heats of ionization were used (Hepes and Tris-HCl), but most experiments were performed at pH 8 in Hepes buffer because of its lower enthalpy of ionization (5.0 and 11.3 kcal·mol$^{-1}$ for Hepes and Tris-HCl at 25 °C, respectively).[54] The thermodynamic data were processed with Origin 7.0 software provided by MicroCal. The values of $\Delta H$ were measured for each titration, and fitting the binding isotherms with a one-site binding model yielded the values of the association constant ($K_a$). The system also gave information of the change in entropy ($\Delta S$). The binding free energy ($\Delta G$) and dissociation constant ($K_d$) were calculated from the experimentally determined values of $\Delta H$ and $K_a$, using eqs 1 and 2:

$$\Delta G = -RT \ln(K_a) = \Delta H - T\Delta S \tag{1}$$

$$K_d = 1/K_a \tag{2}$$

where $R$ is the gas constant (1.987 cal·mol$^{-1}$·K$^{-1}$), and $T$ is the working temperature (298 K). The reported parameters are the average of triplicate measurements. To correct for any discrepancies in the baseline outlined by the software, a manual adjustment was performed. In some cases, the parameter $K_a$ was kept fixed during the refinement to obtain a best fit, expecially at the beginning of the curve.

**Computational Chemistry.** Molecular modeling and graphics manipulations were performed using the molecular operating environment (MOE)[55] and UCSF-CHIMERA software packages,[56] running on a 2 CPU (PIV 2.0−3.0 GHZ) Linux workstation.

**Ligand and Protein Setup.** The core structures of compounds **2** and **4** were constructed using standard bond lengths and bond angles of the MOE fragment library. The carboxylate group was taken as dissociated. Geometry optimizations were accomplished with the MMFF94X force field, available within MOE.

The coordinates of PPARγ in complex with **2** (PDB code: 3R8I) were used in the docking experiments. Bound ligand was removed.

A correct atom assignment for Asn, Gln, and His residues was done, and hydrogen atoms were added using standard MOE geometries. Partial atomic charges were computed by MOE using the AMBER99 force field. All heavy atoms were then fixed, and hydrogen atoms were minimized using the AMBER99 force field and a constant dielectric of 1, terminating at a gradient of 0.001 kcal mol$^{-1}$ Å$^{-1}$.

**Docking Simulations.** Docking of **2** and **4** to PPARγ was performed with GOLD, version 5.0.1,[36] which uses a genetic algorithm for determining the docking modes of ligands and proteins. The binding site was defined as a 13 Å sphere centered on the OH oxygen of Y473 in the PPARγ structure. The Goldscore-CS docking protocol was adopted in this study.[38] In this protocol, the poses obtained with the original GoldScore function were rescored and reranked with the GOLD implementation of the ChemScore function.[38,39] To perform a thorough and unbiased search of the conformation space, each docking run was allowed to produce 200 poses without the option of early termination, using standard default settings. The top solution obtained after reranking of the poses with ChemScore was selected to generate the PPARγ/ligand complexes.

**Protein Expression, Purification, and Crystallization.** The LBD of PPARγ was expressed as N-terminal His-tagged protein using a pET28 vector and purified onto a Ni$^{2+}$-nitriloacetic acid column (GE Healthcare) as previously described.[25] Crystals of apo-PPARγ were obtained by vapor diffusion at 18 °C using a sitting drop made by mixing 2 $\mu$L of protein solution (10 mg·mL$^{-1}$, in 20 mM Tris and 1 mM TCEP, pH 8.0) with 2 $\mu$L of reservoir solution (0.8 M sodium citrate and 0.15 M Tris, pH 8.0). The crystals were soaked for 8 days in a storage solution (1.2 M sodium citrate and 0.15 M Tris, pH 8.0) containing the ligand (0.1 mM). The ligand dissolved in DMSO was diluted in the storage solution so that the final concentration of DMSO was 0.5%. The storage solution with glycerol 20% (v/v) was used as the cryoprotectant. Crystals of PPARγ/**2** belong to the space group C2 with cell parameters shown in Table 1 of the Supporting Information. The asymmetric unit is formed by one homodimer.

**Structure Determination.** X-ray data were collected at 100 K under a nitrogen stream using synchrotron radiation (beamline ID14-1 at ESRF, Grenoble). The diffracted intensities were processed using the programs MOSFLM and SCALA.[57] Structure solution was performed with AMoRe,[58] using the coordinates of PPARγ/**R-1** (PDB code: 2I4J) as a starting model. The coordinates were then refined with CNS.[59] All data between 8−2.3 Å were included. The statistics of crystallographic data and refinement are summarized in Table 1 of the Supporting Information. The coordinates of PPARγ/**2** have been deposited in the Brookhaven Protein Data Bank (PDB) with the code 3R8I.

**Adipogenesis Assay.** The adipogenesis assay was performed as previously described.[60] Briefly, 3T3-L1 cells (American Type Culture Collection, Manassas, VA) were cultured in DMEM supplemented with 10% bovine calf serum. Two days after reaching confluence, differentiation was induced in DMEM supplemented with 10% fetal calf serum and 1 $\mu$M dexamethasone, 0.5 mM 3-isobuthyl-1-methylxanthine (IBMX), and 10 $\mu$g insulin·mL$^{-1}$. After 48 h, cells were supplemented with medium containing 10 $\mu$g insulin·mL$^{-1}$ for an additional four days. Alternatively, cells were differentiated with medium containing 5 $\mu$g insulin·mL$^{-1}$ and 1 $\mu$M rosiglitazone or the other ligands. Medium was replenished with ligands every other day. Lipid content was determined by the staining with Oil Red O. Pictures were taken with an Axiovert 200 microscope at 20× magnification. The quantitation of the intracellular dye was performed after extraction by isopropanol and by reading the absorbance at 550 nm.

**Gene Expression in 3T3-L1 Adipocytes.** Total RNA was extracted from 3T3-L1 adipocytes with Trizol (Sigma, Milano, Italy) followed by purification on RNeasy cartridges (Qiagen, Milano, Italy) according to the manufacturer's instructions. One microgram of total RNA was used to quantitate the mRNA levels of Fabp4, Glut4, and Acrp30 by real time qPCR using a one-step kit with Taqman probes (Bio-Rad Laboratories, Milano, Italy) in a CFX 384 thermal cycler (Bio-Rad). 36B4 was used as the house keeping gene for data normalization. The primer sequences were mouse Fabp4 forward primer 5′-GGC-GTGGAATTCGATGAA-3′, mouse Fabp4 reverse primer 5′-GCTTGT-CACCATCTCGTT-3′, and mouse Fabp4 Taqman probe 5′-TGAT-GCTCTTCACCTTCCTGTCGT-3′; mouse Glut4 forward primer

5′-TGTCGCTGGTTTCTCCAACTG-3′, mouse Glut4 reverse primer 5′-CCATACGATCCGCAACATACTG-3′, and mouse Glut4 Taqman probe 5′-ACCTGTAACTTCATTGTCGGCATGGGTTT-3′; mouse Acrp30 forward primer 5′-AGGCATCCCAGGACATC-3′, mouse Acrp30 reverse primer 5′-CCTGTCATTCCAACATCTCC-3′, and mouse Acrp30 Taqman probe 5′-CCTTAGGACCAAGAAGACCTGCATCTC-3′; mouse 36B4 forward primer 5′-AGATGCAGCAGATCCGCAT-3′, mouse 36B4 reverse primer 5′-GTTCTTGCCCATCAGCACC-3′, and mouse 36B4 Taqman probe 5′-CGCTCCGAGGGAAGGCCG-3′.

**Animal Studies.** Six weeks old C57Bl/6J male mice (at least 6 animals/group) (Charles River Laboratories, Calco, Italy) were fed a high fat diet containing 45% fat as the calorie source for 16 weeks. PPAR ligands were administered once a day for 2 weeks by oral gavage in 0.5% hypromellose (Sigma Aldrich). In a preliminary study, different doses for each compound were tested, and the optimal dosage for compound **R-1** and **S-1** was 10 mg/kg/day and 25 mg/kg/day, respectively. Fenofibrate (100 mg/kg/day) and rosiglitazone (10 mg/kg/day) were used as reference compounds for PPAR$\alpha$ and $\gamma$ activation, respectively. At sacrifice, blood was taken for the determination of biochemical parameters and circulating hormones. Body weight was measured, and the livers of mice were weighed at the end of the experiment and snap frozen in liquid nitrogen for gene expression analysis. Total plasma cholesterol, triglycerides, NEFA, and glucose were measured with standard commercial kits (for cholesterol, Horiba ABX, Roma, Italy; for triglycerides and glucose, Sentinel Diagnostics, Milano, Italy; for NEFA Wako, Neuss, Germany). Insulin levels were determined with ELISA kit (Mercodia, Uppsala Sweden).

All animal studies were approved by the local ethical committee and followed the Italian and European Community legislation.

**In Vivo Magnetic Resonance Imaging of Adipose Tissues.** At day 12 of treatment with ligands, mice underwent in vivo magnetic resonance imaging (MRI) analysis to monitor total body fat distribution during treatments. Mice were anesthetized with 1% isoflurane and were analyzed in a 4.7 T Avance II MRI scanner (Bruker Corporation, Karlsrhue, Germany). After a gradient echo scout, 16 axial 1 mm thick T1 weighted slices were placed in the abdominal region spanning from kidneys to bladder included. The field of view was 30 × 30 mm$^2$ with a matrix of 128 × 128 pixels. Four averages of a spin echo sequence with TE = 10 ms and TR = 400 ms were acquired in 3′25″ and provided a very good contrast between fat and other tissues. In order to maximize consistency between different animals, the slice immediately frontal with respect to the ilium bone was chosen for visceral fat estimation and was computed as (fat area)/(slice area). Areas were semiautomatically delimited and measured with Adobe Photoshop CS3 (Adobe Systems Inc., San Jose, California).

**Oral Glucose Tolerance Test, Insulin Tolerance Test, and the Calculation of the HOMA-IR Index.** For the oral glucose tolerance test (OGTT), mice were fasted overnight and were administered 2 g glucose·kg$^{-1}$ per os. Blood was taken from the tail at 15 min intervals, and glucose concentration was determined with a OneTouch Ultra glucometer (LifeScan, Milano, Italy). For the insulin tolerance test (ITT), mice were fasted six hours and were administered 0.6 IU·kg$^{-1}$ of insulin (Eli Lilly, Firenze, Italy) with an intraperitoneal injection. Blood samples were taken from the tail at 15 min intervals, and glucose concentration was determined with a OneTouch Ultra glucometer (LifeScan).

The homeostatic model assessment of insulin resistance (HOMA-IR) was calculated with the formula

$$\frac{\text{FPI} \times \text{FPG}}{22.5 \times 18}$$

where FPI is the fasting plasma insulin concentration ($\mu$U·mL$^{-1}$), and FPG is the fasting plasma glucose concentration (mg·dL$^{-1}$).

**Gene Expression in the Liver.** Total RNA from the livers of mice treated with the indicated ligands was extracted with Trizol (Sigma, Milano, Italy) followed by purification on RNeasy cartridges (Qiagen, Milano, Italy) according to the manufacturer's instructions. One microgram of total RNA was used to quantitate the mRNA levels

of Acadm, Acadl, and Acox1 by real time qPCR using a one-step kit with Taqman probes (Bio-Rad Laboratories, Milano, Italy) in a CFX 384 thermal cycler (Bio-Rad). 36B4 was used as house keeping gene for data normalization. The primer sequences were mouse Acadm forward primer 5′-ACCCAGATCCTAAAGTACCC-3′, mouse Acadm reverse primer 5′-CGAAAGCAATTCCTCTGGTG-3′, and mouse Acadm Taqman probe 5′-TGGCCCATGTTTAGTTCCTTTTTTCCAA-3′; mouse Acadl forward primer 5′-GAAACCAGGAACTACGTGAAG-3′, mouse Acadl reverse primer 5′-GCTGTCCACAAAAGCTCT-3′, and mouse Acadl Taqman probe 5′-CACACATACAGACGGTGCAGCATA-3′; mouse Acox1 forward primer 5′-TCACGTTTACCCCGGC-3′, mouse Acox1 reverse primer 5′-CAAGTACGACACCATACCAC-3′, and mouse Acox1 Taqman probe 5′-CATCAAGAACCTGGCCGTCTGC-3′; and mouse 36B4 forward primer 5′-AGATGCAGCAGATCCGCAT-3′, and mouse 36B4 reverse primer 5′-GTTCTTGCCCATCAGCACC-3′, and mouse 36B4 Taqman probe 5′-CGCTCCGAGGGAAGGCCG-3′.

**Statistical Analyses.** Statistical analyses were performed via one-way ANOVA with post-test analysis for multiple group comparisons, using GraphPad Prism, version 5.0 (GraphPad Software, San Diego, CA). Differences with $p$ values less than 0.05 were considered statistically significant.

**Effects on Cell Proliferation.** Compound **6** and troglitazone were purchased from Cayman Chemical (Ann Arbor, MI, USA). Stock solutions of these ligands as well as our ureidofibrate-like compounds were prepared at 20 mM in DMSO and stored in aliquots at −20 °C.

**Cell Lines.** Our in vitro model was made up of HT-29 colon adenocarcinoma, LoVo, and HCT15 metastatic colon adenocarcinoma.

**Evaluation of Cytotoxicity.** Determination of the IC$_{50}$ was performed using the 3-[4,5-dimethylthiazol-2-yl]-2,5-diphenyltetrazolium bromide (MTT) assay. On day 1, 10,000 cells/well in a volume of 200 $\mu$L were seeded in 96-wells plates. In each plate, one column contained cells not exposed to drugs (control), and 5 columns contained cells exposed to increasing concentrations of drugs. Each drug was repeated in 6 identical wells. On day 2, ligands (1, 5, 10, 50, and 100 $\mu$M) were added with different times of drug exposure (1 and 2 days). For each drug, results were expressed as dose−effect curves with a plot of the fraction of unaffected (surviving) cells versus drug concentration. The IC$_{50}$ value was defined as the drug concentration yielding a fraction of affected (no surviving) cells = 0.5, compared with that of untreated controls and calculated using Calcusyn software. Each experiment was done in triplicate.

**Western Blot Analysis.** Total proteins were extracted from cell culture by homogenization in a radioimmunoprecipitation assay (RIPA) buffer (0.5 M NaCl, 1% Triton X-100, 0.5% NP40, 1% deoxycholic acid, and 3.5 mM sodium dodecyl sulfate (SDS)), with 20% protease inhibitor cocktail (Sigma, Missouri, USA) and measured by the Bradford method. Total cellular proteins were separated by electrophoresis on 8% SDS−polyacrylamide gel and electro-transferred onto PVDF membranes. Membranes were then incubated with the primary antibody. PPAR$\gamma$ monoclonal antibody was from Cayman Chemical (Ann Arbor, MI, USA), and $\beta$-actin monoclonal antibody was from Sigma-Aldrich (Missouri, USA). Membranes were then probed with horseradish peroxidase-labeled secondary antibody, and the signal was detected by the ECL chemoluminescence assay from Amersham Pharmacia Biotech (Uppsala, Sweden). Expression level was evaluated by densitometric analysis using Quantity One software (Bio-Rad, Hercules, CA, USA), and the $\beta$-actin expression level was used to normalize the sample values.

**Cell Cycle Analysis.** Cells were exposed to the ureidofibrate-like enantiomers **R-1** and **S-1**, troglitazone (1, 5, 10, 50, and 100 $\mu$M), or **6** (20 $\mu$M) for 1−2 days. Cells were harvested, washed twice in ice-cold PBS (pH 7.4), fixed in 4.5 mL of 70% ethanol at −20 °C, then washed once in ice-cold PBS. The pellet was resuspended in PBS containing 1 mg·mL$^{-1}$ RNase and 0.01% NP40, and the cellular DNA was stained with 50 $\mu$g·mL$^{-1}$ propidium iodide (Sigma, Missouri, USA). Cells were stored in ice for 30 min prior to analysis. Cell cycle determinations were carried out using a FACScan Flow Cytometer (Becton Dickinson), and data were interpreted using the CellQuest software, provided by the manufacturer.

**Apoptosis Determination.** Exponentially growing cells were treated with drug IC$_{50}$ concentrations for one and two days and then

harvested and centrifuged at 1,200 rpm for 10 min. The supernatant was discarded, and the cell pellets were washed in ice-cold PBS and resuspended in 500 $\mu$L of ice-cold 1× binding buffer (0.1 M Hepes/NaOH, pH 7.4, 1.4 M NaCl, 25 mM CaCl$_2$). Annexin staining was performed according to the manufacturer's protocol (annexin V-FITC apoptosis detection kit I, Becton Dickinson). Cells were stained by the addition of both 5 $\mu$L of annexin V-FITC and 5 $\mu$L of propidium iodide (PI) solution. The annexin V assay allows one to detect apoptosis at a very early stage. This assay takes advantage of the fact that phosphatidylserine (PS), which has a strong, specific affinity for annexin V, is translocated from the inner (cytoplasmic) leaflet of the plasma membrane to the outer (cell surface) leaflet soon after the induction of apoptosis. PS on the outer leaflet is, therefore, available to bind labeled annexin V.[61] Typically, 10,000 events are collected using excitation/emission wavelengths of 488/525 and 488/675 nm for annexin V and PI, respectively. The samples were analyzed with FACScan Flow Cytometer and results carried out using CellQuest software (Becton Dickinson).

**Data Analysis and Presentation.** Each experiment has been repeated three times. All results shown are expressed as the mean plus SD. Significance of the differences has been evaluated by the Student's $t$ test. Differences were considered significant when $p < 0.05$.

## ASSOCIATED CONTENT

### S Supporting Information

Physicochemical properties and spectroscopic data for intermediates and final compounds; statistics of crystallographic data and refinement; superposition of the crystal and docked structure of **2**; activity of **R-1** and **S-1** enantiomers toward PPAR$\alpha$. This material is available free of charge via the Internet at http://pubs.acs.org.

### Abbreviations Used

PPAR, peroxisome proliferator-activated receptor; NEFA, nonesterified fatty acids; OGTT, oral glucose tolerance test; ITT, insulin tolerance test; HOMA-IR, homeostatic model assessment of insulin resistance; PPRE, peroxisome proliferator response elements; SPPARM, selective peroxisome proliferator-activated receptor modulator; NR, nuclear receptor; TZDs, thiazolidinediones; LBD, ligand binding domain; RXR, retinoid X receptor; HOBT, hydroxybenzotriazole; DIC, *N,N*-diisopropylcarbodiimide; DSC, differential scanning calorimetry; ITC, isothermal titration calorimetry; HFD, high fat diet; WAT, white adipose tissue; MRI, magnetic resonance imaging; MOE, molecular operating environment; RIPA, radioimmunoprecipitation assay; RMSF, root-mean-square fluctuation

### Accession Codes

PDB ID: 2I4P; 2I4J; 3R8I.

## AUTHOR INFORMATION

### Corresponding Author

*(M.C.) Phone: +39 02-50318393. Fax: +39 02-50318391. E-mail: maurizio.crestani@unimi.it. (F.L.) Phone: +39 080-5442798. Fax: +39 080-5442231. E-mail: floiodice@farmchim.uniba.it.

### Present Address

▽University of Lausanne, Center for Integrative Genomics, Genopode Building, Room 5010, 1015 Lausanne, Switzerland.

### Author Contributions

○These authors contributed equally to this work.

## REFERENCES

(1) Berger, J. P.; Akiyama, T. E.; Meinke, P. T. PPARs: therapeutic targets for metabolic disease. *Trends Pharmacol. Sci.* **2005**, *26*, 244−251.

(2) Berger, J.; Moller, D. E. The mechanisms of action of PPARs. *Annu. Rev. Med.* **2002**, *53*, 409−435.

(3) Kliewer, S. A.; Sundseth, S. S.; Jones, S. A.; Brown, P. J.; Wisely, G. B.; Koble, C. S.; Devchand, P.; Wahli, W.; Willson, T. M.; Lenhard, J. M.; Lehmann, J. M. Fatty acids and eicosanoids regulate gene expression through direct interactions with peroxisome proliferator-activated receptors alpha and gamma. *Proc. Natl. Acad. Sci. U.S.A.* **1997**, *94*, 4318−4323.

(4) Nolte, R. T.; Wisely, G. B.; Westin, S.; Cobb, J. E.; Lambert, M. H.; Kurokawa, R.; Rosenfeld, M. G.; Willson, T. M.; Glass, C. K.; Milburn, M. V. Ligand binding and co-activator assembly of the peroxisome proliferatoractivated receptor-gamma. *Nature* **1998**, *395*, 137−143.

(5) Gampe, R. T. Jr.; Montana, V. G.; Lambert, M. H.; Miller, A. B.; Bledsoe, R. K.; Milburn, M. V.; Kliewer, S. A.; Willson, T. M.; Xu, H. E. Asymmetry in the PPAR[gamma]/RXR[alpha] crystal structure reveals the molecular basis of heterodimerization among nuclear receptors. *Mol. Cell* **2000**, *5*, 545−555.

(6) Willson, T. M.; Brown, P. J.; Sternbach, D. D.; Henke, B. R. The PPARs: from orphan receptors to drug discovery. *J. Med. Chem.* **2000**, *43*, 527−550.

(7) Evans, R. M.; Barish, G. D.; Wang, Y. X. PPARs and the complex journey to obesity. *Nat. Med.* **2004**, *10*, 355−361.

(8) Semple, R. K.; Chatterjee, V. K.; O'Rahilly, S. PPAR gamma and human metabolic disease. *J. Clin. Invest.* **2006**, *116*, 581−589.

(9) Schoonjans, K.; Auwerx, J. Thiazolidinediones: an update. *Lancet* **2000**, *355*, 1008−1010.

(10) Nesto, R. W.; Bell, D.; Bonow, R. O.; Fonseca, V.; Grundy, S. M.; Horton, E. S.; Le Winter, M.; Porte, D.; Semenkovich, C. F.; Smith, S.; Young, L. H.; Kahn, R. Thiazolidinedione use, fluid retention, and congestive heart failure: a consensus statement from the American Heart Association and American Diabetes Association. *Diabetes Care* **2004**, *27*, 256−263.

(11) Bodmer, M.; Meier, C.; Kraenzlin, M. E.; Meier, C. R. Risk of fractures with glitazones: a critical review of the evidence to date. *Drug. Saf.* **2009**, *32*, 539−547.

(12) Rocchi, S.; Picard, F.; Vamecq, J.; Gelman, L.; Potier, N.; Zeyer, D.; Dubuquoy, L.; Bac, P.; Champy, M. F.; Plunket, K. D.; Leesnitzer, L. M.; Blanchard, S. G.; Desreumaux, P.; Moras, D.; Renaud, J. P.; Auwerx, J. A unique PPARgamma ligand with potent insulin-sensitizing yet weak adipogenic activity. *Mol. Cell* **2001**, *8*, 737−747.

(13) Berger, J. P.; Petro, A. E.; Macnaul, K. L.; Kelly, L. J.; Zhang, B. B.; Richards, K.; Elbrecht, A.; Johnson, B. A.; Zhou, G.; Doebber, T. W.; Biswas, C.; Parikh, M.; Sharma, N.; Tanen, M. R.; Thompson, G. M.; Ventre, J.; Adams, A. D.; Mosley, R.; Surwit, R. S.; Moller, D. E. Distinct properties and advantages of a novel peroxisome proliferator-activated protein [gamma] selective modulator. *Mol. Endocrinol.* **2003**, *17*, 662−676.

(14) Misra, P.; Chakrabarti, R.; Vikramadithyan, R. K.; Bolusu, G.; Juluri, S.; Hiriyan, J.; Gershome, C.; Rajjak, A.; Kashireddy, P.; Yu, S.; Surapureddi, S.; Qi, C.; Zhu, Y. J.; Rao, M. S.; Reddy, J. K.; Ramanujam, R. PAT5A: a partial agonist of peroxisome proliferator-activated receptor gamma is a potent antidiabetic thiazolidinedione yet weakly adipogenic. *J. Pharmacol. Exp. Ther.* **2003**, *306*, 763−771.

(15) Minoura, H.; Takeshita, S.; Ita, M.; Hirosumi, J.; Mabuchi, M.; Kawamura, I.; Nakajima, S.; Nakayama, O.; Kayakiri, H.; Oku, T.; Ohkubo-Suzuki, A.; Fukagawa, M.; Kojo, H.; Hanioka, K.; Yamasaki,

N.; Imoto, T.; Kobayashi, Y.; Mutoh, S. Pharmacological characteristics of a novel nonthiazolidinedione insulin sensitizer, FK614. *Eur. J. Pharmacol.* **2004**, *494*, 273−281.

(16) Acton, J. J. III; Black, R. M.; Jones, A. B.; Moller, D. E.; Colwell, L.; Doebber, T. W.; Macnaul, K. L.; Berger, J.; Wood, H. B. Benzoyl 2-methyl indoles as selective PPARgamma modulators. *Bioorg. Med. Chem. Lett.* **2005**, *15*, 357−362.

(17) Dropinski, J. F.; Akiyama, T.; Einstein, M.; Habulihaz, B.; Doebber, T.; Berger, J. P.; Meinke, P. T.; Shi, G. Q. Synthesis and biological activities of novel aryl indole-2-carboxylic acid analogs as PPARgamma partial agonists. *Bioorg. Med. Chem. Lett.* **2005**, *15*, 5035−5038.

(18) Reifel-Miller, A.; Otto, K.; Hawkins, E.; Barr, R.; Bensch, W. R.; Bull, C.; Dana, S.; Klausing, K.; Martin, J. A.; Rafaeloff-Phail, R.; Rafizadeh-Montrose, C.; Rhodes, G.; Robey, R.; Rojo, I.; Rungta, D.; Snyder, D.; Wilbur, K.; Zhang, T.; Zink, R.; Warshawsky, A.; Brozinick, J. T. A peroxisome proliferator-activated receptor alpha/gamma dual agonist with a unique in vitro profile and potent glucose and lipid effects in rodent models of type 2 diabetes and dyslipidemia. *Mol. Endocrinol.* **2005**, *19*, 1593−1605.

(19) Martín, J. A.; Brooks, D. A.; Prieto, L.; González, R.; Torrado, A.; Rojo, I.; López de Uralde, B.; Lamas, C.; Ferreto, R.; Dolores Martín-Ortega, M.; Agejas, J.; Parra, F.; Rizzo, J. R.; Rhodes, G. A.; Robey, R. L.; Alt, C. A.; Wendel, S. R.; Zhang, T. Y.; Reifel-Miller, A.; Montrose-Rafizadeh, C.; Brozinick, J. T.; Hawkins, E.; Misener, E. A.; Briere, D. A.; Ardecky, R.; Fraser, J. D.; Warshawsky, A. M. 2-Alkoxydihydrocinnamates as PPAR agonists. Activity modulation by the incorporation of phenoxy substituents. *Bioorg. Med. Chem. Lett.* **2005**, *15*, 51−55.

(20) Burgermeister, E.; Schnoebelen, A.; Flament, A.; Benz, J.; Stihle, M.; Gsell, B.; Rufer, A.; Ruf, A.; Kuhn, B.; Märki, H. P.; Mizrahi, J.; Sebokova, E.; Niesor, E.; Meyer, M. A novel partial agonist of peroxisome proliferator-activated receptor-gamma (PPARgamma) recruits PPARgamma-coactivator-1alpha, prevents triglyceride accumulation, and potentiates insulin signaling in vitro. *Mol. Endocrinol.* **2006**, *20*, 809−830.

(21) Allen, T.; Zhang, F.; Moodie, S. A.; Clemens, L. E.; Smith, A.; Gregoire, F.; Bell, A.; Muscat, G. E.; Gustafson, T. A. Halofenate is a selective peroxisome proliferator-activated receptor gamma modulator with antidiabetic activity. *Diabetes* **2006**, *55*, 2523−2533.

(22) Carmona, M. C.; Louche, K.; Lefebvre, B.; Pilon, A.; Hennuyer, N.; Audinot-Bouchez, V.; Fievet, C.; Torpier, G.; Formstecher, P.; Renard, P.; Lefebvre, P.; Dacquet, C.; Staels, B.; Casteilla, L.; Pénicaud, L. S 26948: a new specific peroxisome proliferator activated receptor gamma modulator with potent antidiabetes and antiatherogenic effects. *Diabetes* **2007**, *56*, 2797−2808.

(23) Kim, M. K.; Chae, Y. N.; Kim, H. S.; Choi, S. H.; Son, M. H.; Kim, S. H.; Kim, J. K.; Moon, H. S.; Park, S. K.; Shin, Y. A.; Kim, J. G.; Lee, C. H.; Lim, J. I.; Shin, C. Y. PAR-1622 is a selective peroxisome proliferator-activated receptor gamma partial activator with preserved antidiabetic efficacy and broader safety profile for fluid retention. *Arch. Pharm. Res.* **2009**, *32*, 721−727.

(24) Motani, A.; Wang, Z.; Weiszmann, J.; McGee, L. R.; Lee, G.; Liu, Q.; Staunton, J.; Fang, Z.; Fuentes, H.; Lindstrom, M.; Liu, J.; Biermann, D. H.; Jaen, J.; Walker, N. P.; Learned, R. M.; Chen, J. L.; Li, Y. INT131: a selective modulator of PPAR gamma. *J. Mol. Biol.* **2009**, *386*, 1301−1311.

(25) Pochetti, G.; Godio, C.; Mitro, N.; Caruso, D.; Galmozzi, A.; Scurati, S.; Loiodice, F.; Fracchiolla, G.; Tortorella, P.; Laghezza, A.; Lavecchia, A.; Novellino, E.; Mazza, F.; Crestani, M. Insights into the mechanism of partial agonism: crystal structures of the peroxisome proliferator-activated receptor gamma ligand-binding domain in the complex with two enantiomeric ligands. *J. Biol. Chem.* **2007**, *282*, 17314−17324.

(26) Pochetti, G.; Mitro, N.; Lavecchia, A.; Gilardi, F.; Besker, N.; Scotti, E.; Aschi, M.; Re, N.; Fracchiolla, G.; Laghezza, A.; Tortorella, P.; Montanari, R.; Novellino, E.; Mazza, F.; Crestani, M.; Loiodice, F. Structural insight into peroxisome proliferator-activated receptor $\gamma$ binding of two ureidofibrate-like enantiomers by molecular dynamics, cofactor interaction analysis, and site-directed mutagenesis. *J. Med. Chem.* **2010**, *53*, 4354−4366.

(27) Sarraf, P.; Muller, E.; Jones, D.; Holden, S.; Tomoyasu, S.; Koeffler, H. P. Differentiation and reversal of malignant changes in colon cancer through PPAR$\gamma$ differentiation. *Nat. Med.* **1998**, *4*, 1046−1052.

(28) Hisatake, J. I.; Ikezoe, T.; Carey, M.; Holden, S.; Tomoyasu, S.; Koeffler, H. P. Downregulation of prostate-specific antigen expression by ligands for peroxisome proliferator-activated receptor $\gamma$ in human prostate cancer. *Cancer Res.* **2000**, *60*, 5494−5498.

(29) Liu, H.; Zang, C.; Fenner, M. H.; Possinger, K.; Elstner, E. PPAR gamma ligands and ATRA inhibit the invasion of human breast cancer cells in vitro. *Breast Cancer Res. Treat.* **2003**, *79*, 63−74.

(30) Grommes, C.; Landreth, G. E.; Heneka, M. T. Antineoplastic effects of peroxisome proliferator-activated receptor gamma agonists. *Lancet Oncol.* **2004**, *5*, 419−429.

(31) Theocharis, S.; Margeli, A.; Vielh, P.; Kouraklis, G. Peroxisome proliferator-activated receptor-gamma ligands as cell-cycle modulators. *Cancer Treat. Rev.* **2004**, *30*, 545−554.

(32) Pinelli, A.; Godio, C.; Laghezza, A.; Mitro, N.; Fracchiolla, G.; Tortorella, V.; Lavecchia, A.; Novellino, E.; Fruchart, J. C.; Staels, B.; Crestani, M.; Loiodice, F. Synthesis, biological evaluation, and molecular modeling investigation of new chiral fibrates with PPARalpha and PPARgamma agonist activity. *J. Med. Chem.* **2005**, *48*, 5509−5519.

(33) Fracchiolla, G.; Laghezza, A.; Piemontese, L.; Carbonara, G.; Lavecchia, A.; Tortorella, P.; Crestani, M.; Novellino, E.; Loiodice, F. Synthesis, biological evaluation, and molecular modeling investigation of chiral phenoxyacetic acid analogues with PPARalpha and PPARgamma agonist activity. *ChemMedChem* **2007**, *2*, 641−654.

(34) Fracchiolla, G.; Lavecchia, A.; Laghezza, A.; Piemontese, L.; Trisolini, R.; Carbonara, G.; Tortorella, P.; Novellino, E.; Loiodice, F. Synthesis, biological evaluation, and molecular modeling investigation of chiral 2-(4-chloro-phenoxy)-3-phenyl-propanoic acid derivatives with PPARalpha and PPARgamma agonist activity. *Bioorg. Med. Chem.* **2008**, *16*, 9498−9510.

(35) Fracchiolla, G.; Laghezza, A.; Piemontese, L.; Tortorella, P.; Mazza, F.; Montanari, R.; Pochetti, G.; Lavecchia, A.; Novellino, E.; Pierno, S.; Conte Camerino, D.; Loiodice, F. New 2-aryloxy-3-phenyl-propanoic acids as peroxisome proliferator-activated receptors alpha/gamma dual agonists with improved potency and reduced adverse effects on skeletal muscle function. *J. Med. Chem.* **2009**, *52*, 6382−6393.

(36) (a) *GOLD*, version 5.0.1; CCDC Software Limited: Cambridge, U.K., 2008. (b) Jones, G.; Willett, P.; Glen, R. C.; Leach, A. R.; Taylor, R. Development and validation of a genetic algorithm for flexible docking. *J. Mol. Biol.* **1997**, *267*, 727−748.

(37) (a) Schulz-Gasch, T.; Stahl, M. Binding site characteristics in structure-based virtual screening: evaluation of current docking tools. *J. Mol. Model* **2003**, *9*, 47−57. (b) Wang, R.; Lu, Y.; Wang, S. Comparative evaluation of 11 scoring functions for molecular docking. *J. Med. Chem.* **2003**, *46*, 2287−2303. (c) Kellenberger, E.; Rodrigo, J.; Muller, P.; Rognan, D. Comparative evaluation of eight docking tools for docking and virtual screening accuracy. *Proteins: Struct., Funct., Bioinf.* **2004**, *57*, 225−242. (d) Warre, G. L.; Andrews, C. W.; Capelli, A. M.; Clarke, B.; LaLonde, J.; Lambert, M. H.; Lindvall, M.; Nevins, N.; Semus, S. F.; Senger, S.; Tedesco, G.; Wall, I. D.; Woolven, J. M.; Peishoff, C. E.; Head, M. S. A critical assessment of docking programs and scoring functions. *J. Med. Chem.* **2006**, *49*, 5912−5931.

(38) Verdonk, M. L.; Cole, J. C.; Hartshorn, M. J.; Murray, C. W.; Taylor, R. D. Improved protein-ligand docking using GOLD. *Proteins: Struct., Funct., Genet.* **2003**, *52*, 609−623.

(39) Eldridge, M. D.; Murray, C. W.; Auton, T. R.; Paolini, G. V.; Mee, R. P. Empirical scoring functions: I. The development of a fast empirical scoring function to estimate the binding affinity of ligands in receptor complexes. *J. Comput.-Aided Mol. Des.* **1997**, *11*, 425−445.

(40) Rubenstrunk, A.; Hanf, R.; Hum, D. W.; Fruchart, J.-C.; Staels, B. Safety issues and prospects for future generations of PPAR modulators. *Biochim. Biophys. Acta* **2007**, *1771*, 1065−1081.

(41) Peraza, M. A.; Burdick, A. D.; Marin, H. E.; Gonzalez, F. J.; Peters, J. M. The toxicology of ligands for peroxisome proliferator-activated receptors (PPAR). *Toxicol. Sci.* **2006**, *90*, 269−295.

(42) Cheung, C.; Akiyama, T. E.; Ward, J. M.; Nicol, C. J.; Feigenbaum, L.; Vinson, C.; Gonzalez, F. J. Diminished hepatocellular proliferation in mice humanized for the nuclear receptor peroxisome proliferator-activated receptor α. *Cancer Res.* **2004**, *64*, 3849−3854.

(43) Després, J.-P.; Lemieux, I. Abdominal obesity and metabolic syndrome. *Nature* **2006**, *444*, 881−887.

(44) Kahn, S. E.; Hull, R. L.; Utzschneider, K. M. Mechanisms linking obesity to insulin resistance and type 2 diabetes. *Nature* **2006**, *444*, 840−846.

(45) Heikkinen, S.; Argmann, C. A.; Champy, M.-F.; Auwerx, J. Evaluation of glucose homeostasis. *Curr. Protoc. Mol. Biol.* **2007**, 29B.3.1−29B.3.22.

(46) Shearer, B. G.; Billin, A. N. The next generation of PPAR drugs: Do we have the tools to find them? *Biochim. Biophys. Acta* **2007**, *1771*, 1082−1093.

(47) Nissen, S. E.; K. Wolski, K. Effect of rosiglitazone on the risk of myocardial infarction and death from cardiovascular causes. *N. Engl. J. Med.* **2007**, *356*, 2457−2471.

(48) Mattison, Y. B.; Putten, V. V.; Chan, D.; Winn, R.; Geraci, M. W.; Nemenoff, R. A. Peroxisome proliferator-activated receptor-γ (PPARγ) inhibits tumorigenesis by reversing the undifferentiated phenotype of metastatic non-small-cell lung cancer cells (NSCLC). *Oncogene* **2005**, *24*, 1412−1422.

(49) Leesnitzer, L. M.; Parks, D. J.; Bledsoe, R. K.; Cobb, J. E.; Collins, J. L.; Consler, T. G.; Davis, R. G.; Hull-Ryde, E. A.; Lenhard, J. M.; Patel, L.; Plunket, K. D.; Shenk, J. L.; Stimmel, J. B.; Therapontos, C.; Willson, T. M.; Blanchard, S. G. Functional consequences of cysteine modification in the ligand binding sites of peroxisome proliferator-activated receptors by GW9662. *Biochemistry* **2002**, *41*, 6640−6650.

(50) Seargent, J. M.; Yates, E. A.; Gill, J. H. GW9662, a potent antagonist of PPARγ, inhibits growth of breast tumour cells and promotes the anticancer effects of the PPARγ agonist rosiglitazone, independently of PPARγ activation. *Br. J. Pharmacol.* **2004**, *143*, 933−937.

(51) Raspe, E.; Madsen, L.; Lefebvre, A. M.; Leitersdorf, I.; Gelman, L.; Peinado-Onsurbe, J.; Dallongeville, J.; Fruchart, J.-C.; Berge, R.; Staels, B. Modulation of rat liver apolipoprotein gene expression and serum lipid levels by tetradecylthioacetic acid (TTA) via PPARalpha activation. *J. Lipid Res.* **1999**, *40*, 2099−2110.

(52) Hollon, T.; Yoshimura, F. K. Variation in enzymatic transient gene expression assays. *Anal. Biochem.* **1989**, *182*, 411−418.

(53) Sturtevant, J. M. Biochemical Applications of Differential Scanning Calorimetry. *Annu. Rev. Phys. Chem.* **1987**, *38*, 463−488.

(54) Fukada, H.; Takahashi, K. Enthalpy and heat capacity changes for the proton dissociation of various buffer components in 0.1 M potassium chloride. *Proteins* **1998**, *33*, 159−166.

(55) *Molecular Operating Environment (MOE)*, version 2005.06; Chemical Computing Group, Inc.: Montreal, Canada, 2005.

(56) Huang, C. C.; Couch, G. S.; Pettersen, E. F.; Ferrin, T. E. Chimera: an extensible molecular modelling application constructed using standard components. *Pac. Symp. Biocomput.* **1996**, *1*, 724 http://www.cgl.ucsf.edu/chimera.

(57) Leslie, A. G. W. Recent changes to the MOSFLM package for processing film and image plate data. *Jt. CCP4 ESF-EACMB Newslett. Protein Crystallogr.* **1992**, *26*, 27−33.

(58) Navaza, J. AMoRe: an automated package for molecular replacement. *Acta Crystallogr., Sect. A* **1994**, *50*, 157−163.

(59) Brunger, A. T.; Adams, P. D.; Clore, G. M.; DeLano, W. L.; Gros, P.; Grosse-Kunstleve, R. W.; Jiang, J. S.; Kuszewski, J.; Nilges, M.; Pannu, N. S.; Read, R. J.; Rice, L. M.; Simonson, T.; Warren, G. L. Crystallography NMR system: a new software suite for macromolecular structure determination. *Acta Crystallogr., Sect. D* **1998**, *54*, 905−921.

(60) Rieusset, J.; Touri, F.; Michalik, L.; Escher, P.; Desvergne, B.; Niesor, E.; Wahli, W. A new selective peroxisome proliferator-activated receptor gamma antagonist with antiobesity and antidiabetic activity. *Mol. Endocrinol.* **2002**, *16*, 2628−2644.

(61) Van Engeland, M.; Nieland, L. J. W.; Ramaekers, F. C. S.; Schutte, B.; Reutelingsperger, C. P. M. Annexin V-affinity assay: a review on an apoptosis detection system based on phosphatidylserine exposure. *Cytometry* **1998**, *31*, 1−9.